The effects of 17α-estradiol treatment on endocrine system revealed by single-nucleus transcriptomic sequencing of hypothalamus

Lei Li[#,*1], Guanghao Wu[#2], Xiaolei Xu[3], Junling Yang[4], Lirong Yi[5], Ziqing Yang[6], Zheng Mo[3], Li Xing[3], Ying Shan[*1], Zhuo Yu[*3], Yinchuan Li[*5]

[1]Department of Obstetrics and Gynecology, National Clinical Research Center for Obstetric & Gynecologic Diseases, Peking Union Medical College Hospital, Chinese Academy of Medical Sciences and Peking Union Medical College, 100730 Beijing, China.

[2]School of Medical Technology，Beijing Institute of Technology, 100081, Beijing, China.

[3]Department of Medical Oncology，Beijing Tsinghua Changgung Hospital, School of Clinical Medicine, Tsinghua University, 102218, Beijing, China.

[4]Department of Cancer Biology and Pharmacology, University of Illinois College of Medicine, Peoria, Illinois, United states of America.

[5]Institute of Reproductive Medicine, Medical School of Nantong University, Nantong, Jiangsu 226001, China.

[6]School of Basic Medical Sciences, Shandong University, Jinan, Shandong 250012, China.

# These authors contributed equally: Lei Li, Guanghao Wu

* Corresponding author. Email: shypumch@163.com; lilei64@pumch.cn; yza02214@btch.edu.cn; 18622397604@163.com

Abstract

In this study, we investigated 17α-estradiol's role in lifespan extension from long-term administration. Pooled hypothalami from aged male Norway brown rats treated with 17α-estradiol (O.T), aged male controls (O), and young male controls (Y) underwent single-nucleus transcriptomic sequencing (snRNA-seq). To evaluate the effects of 17α-estradiol on aging neurons, supervised clustering of neurons based on neuropeptides and their receptors were used to evaluate the responses of each neuron subtype during aging and after 17α-estradiol treatment. The elevated cellular metabolism, stress and decreased expression levels of pathways involved in synapse formation in neurons initiated by aging were significantly attenuated by 17α-estradiol. Assessment

of changes in neuron populations showed that neurons related to food intake, reproduction, blood pressure, stress response, and electrolyte balance were sensitive to 17α-estradiol treatment. 17α-estradiol treatment not only increased serum Oxytocin (Oxt), but also heightened the activity of hypothalamic-pituitary-gonadal (HPG) axis, as evidenced by significantly elevated levels of plasma Gnrh, total testosterone, and decreased estradiol. Elevated Gnrh1 was confirmed to be one of the causal effects mediating the role of 17α-estradiol in energy homeostasis, neural synapse, and stress response. Notably, *Crh* neurons exhibited prominent stressed phenotype in O.T, distinct to appetite-stimulating neurons *Agrp* and *Ghrl*. Therefore, the HPG axis and energy metabolism may be key targets of 17α-estradiol in male hypothalamus. Additionally, supervised clustering of neurons was shown to be a useful method for assessing treatment responses and cellular perturbation among different neuron subtypes in the hypothalamus.

Key words snRNA-seq, hypothalamus, 17α-estradiol, aging, Crh, Oxt, Gnrh

Background

The hypothalamus serves as the central hub for controlling energy homeostasis, stress response, temperature, learning, feeding, sleep, social behavior, sexual behavior, hormone secretion, reproduction, osmoregulation, blood pressure, visceral activities, emotion, and circadian rhythms [1]. The hypothalamic energy-sensing system, particularly the circuits that regulate food intake, plays a crucial role in life span extension [2]. Elevated metabolic activity in the aged hypothalamus has been reported in aged hypothalamus, including increased mTor signaling [3, 4]. Additionally, decreases in gonadotropin-releasing hormone (GnRH), Ghrh, Trh, monoamine neurotransmitters, and blood supply are hallmarks of aging hypothalamus [5].

Previous studies have demonstrated that 17α-estradiol extends the lifespan of male mice and has beneficial effects on metabolism and inflammation, similar to those of rapamycin and acarbose [6-8]. Recent study indicated that 17α-estradiol also extends the lifespan of male rats [9].Further investigations revealed certain unique features of 17α-estradiol in life extension distinct to rapamycin and acarbose [10, 11]. Moreover, it has been shown that 17α-estradiol targets hypothalamic *POMC* neurons to reduce metabolism by decreasing feeding behavior through anorexigenic pathways [12]. Interestingly, the lifespan extension effect has only been observed in male animals [13]. The safety of 17α-estradiol is key for translation into clinical treatment, and the

potential side effects on reproduction and feminization by 17α-estradiol treatment must be considered. However, contradictory results have been reported regarding its side effects on reproduction and feminization [6, 14, 15]. Therefore, further investigation and verification are needed to understand the underlying mechanisms of lifespan extension and the safety of 17α-estradiol.

In this report, we utilized single-nucleus transcriptomic sequencing and performed supervised clustering of neurons based on neuropeptides, hormones, and their receptors. Supervised clustering offers better resolution in cell cluster screening compared to traditional unsupervised clustering. We assessed the effects of 17α-estradiol on metabolism, stress responses, ferroptosis, senescence, inflammation, and pathways involved in synaptic activity in each neuron subtype, ranking the most sensitive neurons. The effects of 17α-estradiol on reversing aging-related cellular processes were evaluated by two opposing regulatory networks involved in hypermetabolism, stress, inflammation, and synaptic activity. Several key endocrine factors from serum were examined, and the potential side effects of 17α-estradiol on specific neurons were also evaluated.

Materials and methods

Animals, treatment and tissues

Twelve Norway brown male rats (12 months old) were acquired from Charles River, including 8 12-months old and 4 1-month old (Beijing). Aged rats were randomly allocated into control and 17α-estradiol-treated groups. Four Aged rats treated with 17α-estradiol (Catalog #: E834897, Macklin Biochemical, Shanghai, China) were fed freely with regular diet mixed with 17α-estradiol at a dose of 14.4 mg/kg (14.4 ppm), starting at 24 months of age for 6 months according to prior reports [16, 17]. The young rats were fed a regular diet without 17α-estradiol continuously for 3 months until 4 months old. All rats had ad libitum access to food and water throughout the experiments. The rats were then euthanized via CO_2, hypothalami, testes and blood serum were collected for subsequent experimental procedures. All blood samples were collected at 9:00-9:30 a.m to minimize hormone fluctuation between animals. All animal procedures were reviewed and approved by the Institutional Animal Care and Use Committee at Nantong University.

Enzyme immunoassays

Enzyme immunoassays kits for rat Oxt (Catalog #: EIAR-OXT), Corticotropin Releasing Factor (Catalog #: EIAR-CRF), and gonadoliberin-1 (Catalog #: EIAR-GNRH) were obtained from Raybiotech (GA, USA). Enzyme immunoassay kits for rat serum total testosterone (Catalog #: ml002868), estradiol (Catalog #: ml002891), aldosterone (Catalog #: ml002876), and cortisol (Catalog #: ml002874) were obtained from Enzyme-linked Biotechnology (Shanghai, China). Sera from 3 animals per group were used and each was diluted 10 or 20 times for immunoassays.

Seminiferous tubule inflammation test

8 testes were obtained from each sample group and then subjected to fixation in 4% formalin for at least 1 week. Formalin-fixed paraffin-embedded rat testis sections of 5 μm thickness were used for HE Staining. At least 30 seminiferous tubules in each slide were examined for inflammation test. Testis with at least 1 inflammatory seminiferous tubule was set as 1, and normal testis was set as 0 for inflammation index calculation.

snRNA-seq data processing, batch effect correction, and cell subset annotation

Intact hypothalami were cryopreserved in liquid nitrogen from sacrificed rats. Two (O) or three (Y and O.T) hypothalami were pooled within each group and homogenized in 500 μL ice-cold homogenization buffer (0.25 M sucrose, 5 mM $CaCl_2$, 3 mM $MgAc_2$, 10 mM Tris-HCl [pH 8.0], 1 mM DTT, 0.1 mM EDTA, 1× protease inhibitor, and 1 U/μL RiboLock RNase inhibitor) with Dounce homogenizer. Then, the homogenizer was washed with 700 μL ice-cold nuclei washing buffer (0.04% bovine serum albumin, 0.2 U/μL RiboLock RNase Inhibitor, 500 mM mannitol, 0.1 mM phenylmethanesulfonyl fluoride protease inhibitor in 1× phosphate buffer saline). Next, the homogenates were filtered through a 70-μm cell strainer to collect the nuclear fraction. The nuclear fraction was mixed with an equal volume of 50% iodixanol and added on top of a 30% and 33% iodixanol gradient. This solution was then centrifuged for 20 min at 10 000 ×g at 4 °C. After the myelin layer was removed from the top of the gradient, the nuclei were collected from the 30% and 33% iodixanol interface. The nuclei were resuspended in nuclear wash buffer and resuspension buffer and pelleted for 5 min at 500 ×g at 4 °C. The nuclei were filtered through a 40-μm cell strainer to remove cell debris and large clumps, and the nuclear concentration was manually assessed using trypan blue counterstaining and a hemocytometer. Finally, the nuclei were adjusted to 700–1200 nuclei/μL, and examined with a 10X Chromium platform.

Reverse transcription, cDNA amplification and library preparation were performed according to

the protocol from 10X Genomics and Chromium Next GEM Single Cell 3′ Reagent Kits v3.1. Library sequencing was performed on the Illumina HiSeq™ 4000 by Gene Denovo Biotechnology Co., Ltd (Guangzhou, China).

10X Genomics Cell Ranger software (version 3.1.0) was used to convert raw BCL files to FASTQ files, and for alignment and counts quantification. Reads with low-quality barcodes and UMIs were filtered out and then mapped to the reference genome. Reads uniquely mapped to the transcriptome and intersecting an exon at least 50% were considered for UMI counting. Before quantification, the UMI sequences were corrected for sequencing errors, and valid barcodes were identified using the EmptyDrops method. The cell × gene matrices were produced via UMI counting and cell barcodes calling. Cells with an unusually high number of UMIs (≥8000) or mitochondrial gene percent (≥15%) were filtered out. Batch effect correction was performed by harmony.

Pathways, gene signatures, TFs and TF cofactors, cell communication

Gene sets and pathways were derived from Hallmark gene sets of MSigDB collections, the KEGG pathway database, Reactome pathway database, and WikiPathways database, and some ontology terms derived from the Gene Ontology (GO) resource. Mitochondrial pathways were derived from MitoCarta3.0 [18]. Pathways, gene sets, and gene signatures were evaluated with the PercentageFeatureSet function built into R package Seurat. TFs and TF cofactors were obtained from AnimalTFDB 3.0 [19]. TFs and TF cofactors were further filtered with mean counts >0.1.

The ligand–receptor pairs were calculated via R package CommPath [20].

Correlation analysis and ROC analysis

Pearson correlation coefficient was calculated with the linkET package ($p < 0.05$). Fast Wilcoxon rank sum test and auROC analysis was performed with the wilcoxauc function in R package presto. The minimal cell number in either one of the comparing pairs should be no less than 15. Ranks of area under the curve (AUC) values were in descending order. A total of 431 pathways from Hallmark, KEGG and PID databases were used for correlation analysis with MitoCarta OXPHOS subunits in neurons and non-neural cells (**Figure 2—figure supplement 1**). A total of 97 pathways related to synapse activity were derived from GO, including GO cellular components, GO biological processes and GO molecular functions (**Table S1**).

The division of expression level-dependent clusters in each pathway and their gene

signatures

The quarters of the mixed cell populations from O, O.T, and Y hypothalamic neurons were equally divided using the R function fivenum from the R package stats, based on pathway expression levels. Thus, the total number of neurons was evenly divided into four clusters (c1-c4) in terms of cell number. The cell proportions from O.T, O, and Y neurons in each cluster were weighted against the total number of neurons in the three groups. The unique markers of each cluster were calculated using the FindAllMarkers function from the Seurat package. The intersection of the unique markers from the six pathways was obtained for heatmap plotting. Nineteen genes that were highly expressed in c1 were identified as c1.up.signature via the PercentageFeatureSet function in the Seurat package. Twelve genes that were highly expressed in c4 were identified as c4.up.signature. There were no intersecting unique markers in clusters c2 and c3 among the six selected pathways.

TF and pathway activities

The TF resources were derived from CollecTRI, the pathway resource was from PROGENy, and the enrichment scores of TFs and pathways were performed with the Univariate Linear Model (ulm) method according to the pipeline in R package decoupleR [21].

Subtypes of neurons generated by supervised clustering and cell prioritization

Vast majority of these subtypes were clustered by neuropeptides, hormones, and their receptors within all the neurons with the subset function from R package Seurat (the target gene expression level > 0). A total of 209 neuron subtypes were obtained, comprising 104 neuropeptide-secreting or hormone-secreting neurons and 105 neurons expressing a unique neuropeptide receptor or hormone receptor (Table S2). Further groupings may exist within the identified neuron subtypes, and the category of excitatory or inhibitory neurons was not discriminated further. The cell proportion of each neuron subtype was weighted according to the total number of neurons in O.T, O, and Y samples. The mean values ± standard deviation of pathways and gene signatures were performed for each subtype. The top 20 and the bottom 20 items were calculated. The cell type prioritization was performed using the R package Augur, with the subsample_size parameter of the calculate_auc function set to 6 [22]. In each comparison pair, the minimum number of cells in a subcluster shall not be less than 6 when performing cell prioritization with function calculate_auc.

Differential expression and pathway enrichment analysis

DEGs between groups were identified via FindMarkers (test.use = bimod, min.pct = 0.1, logfc.Threshold = 0.25, avg_diff > 0.1 or < −0.1). DEGs were then enriched in redundant GO terms via WebGestalt and filtered with false discovery rate < 0.05 [23].

Bidirectional Mendelian randomization (MR) study

The protein quantitative trait locus (pQTL) GWAS summary data of 204 human endocrine-related GWAS summary data with European ancestry were obtained from open-access MRC Integrative Epidemiology Unit (IEU) (**Table S4**) [24, 25]. Independent genome-wide significant SNPs for exposure OXT (id:prot-a-2159) or GNRH1 (id: prot-a-1233) were used as instrumental variables with genome-wide significance ($P < 1 \times 10^{-5}$), independence inheritance (r2 < 0.001) without linkage disequilibrium (LD) with each other for MR. For the reverse MR, independent genome-wide significant SNPs from 203 endocrine-related GWAS summary data ($P < 1 \times 10^{-5}$, r2 < 0.001) without LD with each other were obtained as exposures and human GWAS summary data of OXT (id:prot-a-2159) or GNRH1 (id:prot-a-1233) were used as outcomes. Weak instruments less than 10 were discarded via F-statistics.

MR and reverse MR analysis were conducted with method inverse-variance weighting (IVW), MR Egger, Weighted median, Simple mode, and Weighted mode. The screening criteria: all of the odds ratio (OR) values of the 5 methods should be simultaneously either >1 or <1 and the significant p value of IVW was <0.05. The heterogeneity via IVW method and the horizontal pleiotropy were also evaluated with R package TwoSampleMR [26].

Results

The overall changes in aged hypothalamus with or without long-term 17α-estradiol treatment via snRNA-seq profiling

To investigate the hypothalamus as a potential key target of 17α-estradiol's effects on life extension, we performed snRNA-seq on the entire hypothalamus of aged and 17α-estradiol-treated aged Norway brown rats, using the hypothalamus from young adult male rats as a control. We identified 10 major cell types based on specific cell markers of the hypothalamus (**Figure 1A-B**). Notably, the proportions of all non-neural cells changed in O versus Y (**Figure 1C**). For instance, Oligo, OPC, and Micro were found to be increased, while Astro, Tany, Fibro, PTC, and Endo were

decreased in O compared to Y. The proportions of Oligo, OPC, and Micro were also increased in 17α-estradiol-treated aged group (O.T) compared to those in Y. Furthermore, Endo was increased in O.T compared to both Y and O. The proportions of Astro, Tany, Epen, and PTC decreased more in O.T than those in O when compared to Y. These results indicated that 17α-estradiol treatment had extensive effects on the proportions of non-neural cells in hypothalamus.

Cell communication analysis revealed significant changes in the ligand-receptor pairs between neurons and other cell types, particularly in Endo, Fibro, Tany, and Astro (**Figure 1D**). Significant ligand–receptor interactions among neurons also changed in O.T and O groups, especially in O (**Figure 1E**). Notably, among the significant ligand–receptor pairs in neurons, *Bmp2–Acvr1/Acvr2a/Acvr2b/Bmpr*, *Gdf11–Acvr2a/Acvr2b*, *Inhba–Acvr1/Acvr2a/Acvr2b*, *Nrg1/Nrg2/Nrg4–Erbb4*, *Rspo1–Lgr5/Lrp6*, and *Rspo3–Lgr5* were exclusively and significantly increased in neurons of the O group compared to those in O.T and Y, suggesting enhanced TGF superfamily-mediated signaling activity and canonical Wnt signaling during aging. The significantly changed ligand–receptor pairs *Nlgn1–Nrxn1/Nrxn2*, *Nlgn2–Nrxn1/Nrxn2/Nrxn3*, *Nlgn3–Nrxn1/Nrxn2/Nrxn3*, *Nxph1–Nrxn1/Nrxn2/Nrxn3*, *Nxph3–Nrxn1/Nrxn2/Nrxn3*, *Pomc–Oprd1/Oprk1/Oprm1*, and *Vip–Adcyap1r1/Avpr1a/Vipr2* were exclusively increased in neurons of O.T compared to O and Y (**Figure 1E**). These ligand–receptor pairs were associated with synaptic activity, cellular adhesion, the opioid system, and vasodilation, indicating unique roles of 17α-estradiol in restoring certain physiological functions in the aging hypothalamus. The increased *Pomc* signal in O.T neurons aligns with previous reports suggesting that 17α-estradiol treatment decreases food uptake in mice, potentially correlated with *Pomc* neurons (**Figure 1E**) [12].

Gene set enrichment analysis (GSEA) based on DEGs also corroborated the expression profiles related to stress responses and synapse-associated cellular processes in neurons (**Figure 1F**). ROC analysis of significantly differently expressed pathways related to neural synapses, manually selected from Gene Ontology databases, indicated that most top-ranked pathways related to synapses, according to AUC values, were downregulated in aged neurons, while 17α-estradiol treatment reversed this trend (**Figure 1G, Table S1**).

Overall, these findings suggest that 17α-estradiol broadly reshapes cell populations, cellular communication, neuropeptide secretion, and synapse-related cellular processes in the aging

hypothalamus, distinguishing it from both the young hypothalamus and the untreated aged hypothalamus.

The two opposing signaling networks in regulating metabolism and synapse activity, which can be balanced effectively by 17α-estradiol

To monitor the metabolism and neural status affected by 17α-estradiol, we utilized the energy metabolism pathway MitoCarta OXPHOS subunits to calculate the positively or negatively correlated pathways in hypothalamic neurons (**Figure 2—figure supplement 1**). Our findings revealed that energy metabolism and synapse activity represent two opposing regulatory signaling networks in hypothalamic neurons, with 17α-estradiol strongly playing a significant role in balancing these networks (**Figure 2A**). At the core of these opposing signaling pathways are two categories of contrasting TFs (**Figure 2B**). For example, *Calr*, *Clu*, *Peg3*, *Prnp*, *Ndufa13*, *Actb*, *Ywhab*, *Nfe2l1*, *Mtdh*, *Npm1*, *Bex2*, *Aft4*, and *Maged1* were positively correlated with pathways involved in OXPHOS subunits, lysosome function, protein export, mTorc1 signaling, and the unfolded protein response (UPR) in O, O.T and Y neurons, while showing negative correlations with pathways related to ubiquitin-mediated proteolysis, endocytosis, tight junctions, focal adhesion, axon guidance, and MAPK signaling. Additionally, TFs *Myt1l*, *Ctnnd2*, *Tenm4*, *Camta1*, *Med12l*, *Rere*, *Csrnp3*, *Erbb4*, *Jazf1*, *Dscam*, *Klf12*, and *Kdm4c* exhibited opposite correlation patterns with these selected pathways in O, O.T and Y neurons. These TFs may take conserved roles in regulating the two opposing biological processes in hypothalamic neurons.

We then attempted to establish gene signatures to represent these two opposing signaling networks, thereby displaying the cell status of aging and evaluating the effects exerted by 17α-estradiol. To achieve this, we evenly divided the expression levels of each of the six selected pathways from the two opposing signaling networks into four quarters (c1-c4) among the mixed neurons from O, O.T, and Y, calculating the shared unique markers in each quarter (**Figure 2C, D**). From the distribution patterns, we observed that the proportion of neurons in O decreased from c1 to c4 in metabolic pathways (MitoCarta OXPHOS subunits and Hallmark mTorc1 signaling), while this trend was reversed in the opposing signaling pathways (GOBP synapse organization and KEGG MAPK signaling pathway) (**Figure 2C**). In contrast, in Y, this trend was opposite, suggesting the expression levels from the 4 quarters (c1-c4) of the two opposing signaling networks can be used

to monitor aging status. Treatment with 17α-estradiol alleviated this trend or even reversed it in O. We then screened the shared unique markers of each quarter from the six selected pathways in an attempt to establish the gene signatures representing the two opposing signaling networks. Unique markers in c1 (19 genes, c1.up.signature) and c4 (12 genes, c4.up.signature) were identified; however, c2 and c3 lacked unique markers shared by the 6 pathways (**Figure 2D**). Consequently, the 19 genes in c1.up.signature displayed an inversed correlation pattern with the 12 genes in c4.up.signature, indicating the two opposing gene signatures are capable of reflecting the two opposing signaling networks in hypothalamic neurons (**Figure 2E**). Conversely, the balance of the two opposing signaling networks affected by 17α-estradiol in non-neural cell types was less pronounced than in neurons, showing variable effects on non-neural cells (**Figure 2—figure supplement 2**). GOBP pathway enrichment analysis revealed that Micro exhibited lower levels of synapse-related cellular processes in O.T compared to O, which was distinct from the observations in neurons (**Figure 2—figure supplement 3**). Therefore, in this report, we primarily focused on hypothalamic neurons and their responses to aging and 17α-estradiol.

Supervised clustering revealed distinct responses of different subtypes of hypothalamic neurons to aging and 17α-estradiol

The hypothalamus contains numerous neuron subtypes that release various neuropeptides and hormones to regulate fundamental body functions. To differentiate the changes occurring during aging and the effect of 17α-estradiol on each neuron subtype, we performed supervised clustering based on neuropeptides, hormones, or their receptors (**Table S2**) (**Figure 3A**). The cell counts in each neuronal subcluster classified by neuropeptide secretion (neuropeptide-secreting subtypes) and subclusters defined by neuropeptide or hormone receptor expression (receptor-expressing subtypes) were quantified and compared in sample Y (**Figure 3B**). Notably, neurons expressing *Prlr*, *Esr1*, and *Ar* ranked among the top 20 receptor-expressing subtypes across all analyzed neuron populations. The similarity indices among these cell subtypes were further calculated (**Figure 3—figure supplement 1**), revealing high positive correlations in neuron subtypes expressing *Cartpt*, *Nxph4*, *Bdnf*, *Cck*, *Crh*, *Nppa*, *Adcyap1*, and *Penk*, as well as those expressing *Esr1*, *Calcrl*, and *Pth2r*. These similarities may partially reflect cellular overlap between subtypes (**Figure 3—figure supplement 1**).

We next calculated the prioritization of cellular perturbation induced by aging and/or 17α-estradiol treatment across these screened neuron subtypes (**Figure 3C, D**). The *Gnrh1* neuron subtype ranked among the top perturbed neuropeptide-secreting subtypes in both O vs Y and O.T vs Y comparisons (purple arrows). Notably, *Sct* and *Kiss1* neuron subtypes emerged as the top 2 perturbed populations in the O.T vs O analysis (red arrows), highlighting their heightened sensitivity to 17α-estradiol in the aged hypothalamus. Among receptor-expressing subtypes, *Insr* neurons showed the highest sensitivity to perturbation in both O vs Y and O.T vs Y comparisons (purple arrows, **Figure 3D**), while *Adipor2* and *Mlnr* neurons (blue arrows) ranked as the top 2 sensitive subtypes in the O.T vs O analysis. Intriguingly, neurons expressing *Ar* and *Esr1* ranked among the top 20 most perturbed receptor subtypes during aging (O vs Y), but were no longer ranked in this group following treatment (O.T vs Y and O.T vs O comparisons). This indicates that 17α-estradiol administration attenuated age-associated perturbation in these neuronal subtypes (**Figure 3D**).

Differential senescence or stress levels and subtype-specific susceptibility in aged hypothalamic neurons

To gain a deeper understanding of the effects of 17α-estradiol treatment on the aged hypothalamus, we selected 3 gene signatures and 2 gene sets associated with aging, apoptosis, and stress to characterize the differential responses of distinct neuronal subtypes to aging and 17α-estradiol. These neuronal subtypes were then ranked separately based on neuropeptide-secreting subtypes and receptor-expressing subtypes (**Figure 4A, B**).

Neuropeptide-secreting subtypes, such as *Prlh*-, *Sct*-, *Gast*-, *Nppa*-, *Nxph1*-, *Ucn*-, *Pnoc*-, *Galp*-, and *Ghrl*-expressing neurons, were consistently ranked among the top 20 in at least 4 out of the 5 gene signatures or gene sets. These neurons are involved in gastrointestinal function, food intake, hunger, energy homeostasis, water homeostasis, vascular regulation, and pain, suggesting that aging exacerbates senescence or stress in these physiological processes.

In contrast, neurons expressing *Igf2*, *Crh*, *Npy*, *Npw*, *Npff*, *Nmu*, *Agrp*, or *Adipoq* ranked among the bottom 20 in at least four of the five signatures or gene sets. These neuropeptides and hormones are associated with cortical excitability, stress response, food intake, circadian rhythms, fat metabolism, insulin sensitivity, heart rate, and blood pressure. Notably, although

Crh-expressing neurons exhibited high overall cellular perturbation among neuropeptide-secreting subtypes (**Figure 3C**), the relatively lower senescence and stress burden in *Crh*-, *Npy*-, *Npw*-, and *Nmu*-expressing neurons—key mediators of the stress response—compared to other neuronal subtypes represents a defining characteristic of the aged hypothalamus.

Regarding receptor-expressing subtypes, *Mc3r*-, *Sstr1*-, *Kiss1r*-, *Ntsr2*-, *Mlnr*-, *Ntsr1*-, *Npy1r*-, and *Avpr1a*-expressing neurons were consistently among the top 20 in at least 4 of the 5 gene signatures or gene sets. These receptor-expressing subtypes are involved in food intake, neurotransmission, reproduction, gut function, fat metabolism, circadian rhythm, and vasoconstriction, thereby indicating heightened stress in the aging hypothalamus. Conversely, *Glp2r*-, *Lepr*-, *Paqr8*-, and *Npr3*-expressing neurons were among the bottom 20 in at least 4 of the 5 gene signatures or gene sets, with associations to glucose regulation, fat metabolism, progesterone signaling, blood volume, and blood pressure.

Notably, most of the 5 signatures or gene sets in top ranked neurons exhibited alleviated senescence or stress following 17α-estradiol treatment, indicating that such treatment mitigates senescence or stress in these specific neuronal populations (**Figure 4A, B**).

The appetite-controlling neurons and hypothalamic–pituitary–adrenal (HPA) axis were altered by long-term 17α-estradiol treatment in the males

To further investigate the positive effects, potential side effects or compensatory effects of 17α-estradiol treatment, we performed stricter screening by intersecting the top 20 and bottom 20 ranks of the scores of c1-up-signature, ferroptosis gene signature, UPR, Mtorc1 signaling, and OXPHOS subunits (**Figure 5A**). Neurons expressing *Calcb*, *Edn3*, *Ucn*, *Ghrl*, *Nmu*, *Npff*, *Cnp*, and *Agrp* ranked among the bottom 20 in at least 4 out of the 5 gene signatures or gene sets. These neurons are involved in stress responses, vascular activity, appetite regulation, and muscle contraction. Notably, the lower levels of *Agrp*- and *Ghrl*-expressing neurons in the Mitocarta_OXPHOS_subunits signature may also indicate reduced physiological activity of these potent appetite-promoting neurons during 17α-estradiol treatment, which could represent a key clue to its role in lifespan prolongation.

In contrast, neurons expressing *Gast*, *Npb*, *Nppa*, *Crh*, *Scg3*, and *Npw* consistently ranked among the top 20 in at least 4 of the 5 gene signatures or gene sets. These neurons participate in gastrointestinal activity, feeding behavior, stress responses, cardio-renal homeostasis, and

angiogenesis. Of note, the expression pattern of *Crh* neurons in O.T was opposite to that in O (**Figure 4A**). Additionally, the Mitocarta_OXPHOS_subunits score in *Crh* neurons was the highest among all examined neuropeptide-expressing subtypes (**Figure 5A**), which contrasted sharply with those of *Agrp* and *Ghrl* neurons. Additionally, the treatment with 17α-estradiol in O.T also elevated several key metabolic pathways in *Crh* neurons compared to those in Y and O (**Figure 5B**). 17α-estradiol treatment increased the c1-up-signature while simultaneously reducing many pathways associated with synapse activity and the c4-up-signature in *Crh* neurons of O.T, indicating a potent stressed phenotype in *Crh* neuron. In contrast, in *Kiss1* and *Prlh* neurons, the decreased c1-up-signature in O.T implied a lesser extent of stressed phenotype in these neurons compared to *Crh* neurons. The status of Crh neurons in O.T may be associated with elevated TF activities of *Esr2*, *Usf2*, *Hdac5*, *Creb3l1*, *Tfam*, *Preb*, *Pou3f2*, and *Hoxb5* (**Figure 5C**). The aberrant changes in *Crh* neurons were also evidenced by the increased expression of DEGs related to mitochondria-expressed genes and reduced expression of DEGs in the adherens junction pathway in O.T, indicative of higher energetic activity and altered extracellular adhesion in this type of neuron by 17α-estradiol treatment (**Figure 5D**).

Notably, the HPA axis was altered by 17α-estradiol treatment, as evidenced by the elevated cortisol levels in O.T compared to O ($p = 0.078$) (**Figure 5E**). The correlation between elevated cortisol production and the heightened stress in *Crh* neurons by 17α-estradiol treatment needs further investigation. Additionally, as a crucial component of the renin-angiotensin-aldosterone system, the significantly increased serum aldosterone in O.T and its potential role in sodium reabsorption and cardiovascular health also warrant more detailed investigation (**Figure 5E**).

In summary, 17α-estradiol treatment altered the activity of appetite-promoting neurons and the hypothalamic-pituitary-adrenal (HPA) axis in male BN rats, while also inducing enhanced stress responses in *Crh* neurons.

17α-estradiol increased Oxt neuron proportion and secretion and its possible role in mediating the effect of 17α-estradiol on endocrine system

Aging and 17α-estradiol treatment also altered the proportions of various neuron subtypes among O, O.T, and Y (**Figure 6A, B**). The proportions of *Grp*, *Pmch*, *Npb*, *Serpinb9*, *Sstr2*, *Agrp*, *Sstr3*, *Mlnr*, and *Hcrt* neurons ranked in the top 10 in O, while *Oxt*, *Vip*, *Avp*, *Calca*, *Glp2r*, *Tacr1*, *Trh*,

Serping1, *Npff*, and *Npy1r* were in the top 10 in O.T. *Galp*, *Calcrl*, *Ednra*, *Oxt*, *Serpinh1*, *Pomc*, *Cck*, *Crh*, *Tacr1*, and *Kiss1* neurons were among the bottom 10 in O, whereas *Oxtr*, *Galp*, *Agrp*, *Serpinb9*, *Npvf*, *Serpinh1*, *Ednrb*, *Agt*, *Gipr*, and *Pomc* neurons ranked among the bottom 10 in O.T. *Agrp*, *Pomc*, *Oxt*, *Oxtr*, *Gipr*, and *Glp2r* neurons are well-known for their roles in regulating food intake and energy homeostasis. *Agrp* neurons are activated by hunger, while *Pomc* neurons are activated by satiety in the ARC of the hypothalamus. 17α-estradiol treatment effectively elevated the expression levels of the c4.up.signature (blue arrows) and synapse-associated processes in neuron subtypes *Agrp*, *Pomc*, *Oxt* and *Glp2r* in O.T compared to O. This may mitigate the adverse effects of reduced cell populations in Pomc and *Agrp* neurons in aging hypothalamus (**Figure 6C**). This finding indicates a potential role of 17α-estradiol in appetite control, as previously reported [12]. Additionally, 17α-estradiol treatment resulted in elevated proportions of *Vip*, *Avp*, *Npff*, *Calca*, and *Tacr1* neurons, which ranked in the top 10, while the proportions of Agt neurons decreased. These are all associated with blood pressure regulation (**Figure 6—figure supplement 1**). Notably, the proportions of *Oxt* and *Glp2r* neurons, both of which have anorexigenic effects [27, 28], increased in O.T. In addition to the increased number of *Oxt*-positive neurons, the expression level of *Oxt* also rose in O.T. The elevated expression of synapse-related pathways was supported by the increased DEGs in the enriched synaptic membrane pathway in *Oxt* neurons (**Figure 6D**).

More importantly, the serum level of Oxt was significantly elevated in O.T compared to O ($p = 0.04$), yet remained lower than those in Y (**Figure 6E**). Notably, the top TF activities in O.T and O differed markedly from those in Y (**Figure 6F**). The elevated levels of *Hopx* and *Xbp1* may be associated with the response to 17α-estradiol treatment.

Due to the intricate regulatory networks among various endocrine factors, elucidating the causal effect of Oxt on other endocrine factors is quite complex using traditional methods. MR analysis, employing variant SNPs as genetic tools, is advantageous for such task. We performed a bidirectional MR analysis of the GWAS summary data of human plasma OXT and 203 endocrine-related and hypothalamus-related factors, most of which are protein quantitative trait loci (pQTL) data from the IEU (**Table S3**). As an exposure, OXT revealed a significant causal effect on POMC/beta-endorphin (id:prot-a-2327, id:prot-a-2325), glucagon (id:prot-a-1181), GNRH1/Progonadoliberin-1 (id:prot-a-1233), and total testosterone levels

(id:ebi−a−GCST90012112, id:ieu−b−4864) (**Figure 6G**). NPW and CBLN1 were found to be negatively associated with OXT, but the significance of these associations was not found in the reverse MR analysis (**Figure 6—figure supplement 2A, B**).

In contrast, we could not identify significant associations between OXT and estradiol levels (id:ebi-a-GCST90012105, id:ebi-a-GCST90020092, id:ebi-a-GCST90020091, id:ieu-b-4872, id:ieu-b-4873, id:ukb-e-30800_AFR, id:ukb-e-30800_CSA). Interestingly, QRFP, IGF1, AGRP, TAC4, GRP, CLU, BNF, PCSK7, PACAP, ANP, TAC3, CRH, INSL6, and PRL displayed significant associations with OXT in both MR and reverse MR analysis, indicative of their complex causal effects (**Figure 6—figure supplement 2A, B**).

The results suggest that elevated Oxt levels induced by 17α-estradiol may have positive associations with endocrine factors governing feeding behavior, glucose metabolism, male reproduction, and sex hormones. Therefore, OXT may serve as a potential mediator of 17α-estradiol.

17α-estradiol activated HPG axis and the elevated Gnrh also took important roles in mediating the effect of 17α-estradiol on other endocrine factors

Given the sensitivity of GnRH- and sex hormone receptor-expressing neuron subtypes to 17α-estradiol treatment (**Figure 3C, D**), we analyzed their expression profiles alongside representative pathway genes from two opposing signaling networks - those related to metabolism and synapses - such as the c1-up-signature and c4-up-signature (**Figure 7A**). However, neither the c1-up-signature nor the c4-up-signature was up-regulated in *Gnrh1* neuron in the O.T in comparison with Y. *Ar* and *Esr2* neuron displayed decreased level of c1-up-signature in comparison with O. Only in *Esr1* neuron was the c1-up-signature found to be up-regulated. Meanwhile, both *Ar* and *Esr* neurons displayed increased level of c4-up-signature in O.T comparing with O. *Ar*, *Pgr*, and *Esr1* were also among the top 20 of c4-up-signature, suggesting long-term 17α-estradiol treatment did not impose significant stress on hypothalamic neurons expressing these hormone receptors (**Figure 7—figure supplement 1**). But *Gnrh1* and *Crh* neurons were among the bottom 20, indicative of higher cellular stress by long-term 17α-estradiol treatment. However, based on these cellular perturbations, it's difficult to define the precise physiological status of these subtypes of neurons, particularly regarding neuroendocrine activities.

Consequently, we performed enzyme immunoassays of hormones from the serum of O, O.T and Y. The treatment with 17α-estradiol significantly increased the plasma level of Gnrh compared to Y ($p = 0.0099$) and approached significance when compared to O ($p = 0.096$) (**Figure 7B**). More intriguingly, testosterone levels in serum were significantly increased in O.T compared to O ($p = 0.018$) and approached significance when compared to Y ($p = 0.052$). Additionally, the serum estradiol levels were significantly increased in O compared to Y ($p = 0.011$) and significantly decreased in O.T compared to O ($p = 0.019$), suggesting that 17α-estradiol treatment markedly altered the homeostasis of testosterone and estradiol.

Furthermore, most testes from 30-month-old male BN rats exhibited severe age-related inflammation and epithelial collapse of seminiferous tubules (**Figure 7C**). The testes without inflammation in O.T displayed normal morphology. 17α-estradiol treatment slightly decreased the testis inflammation in O.T compared to that in O ($p = 0.15$), indicating a potential positive role of 17α-estradiol treatment in male reproductive system. The elevated TFs such as *Sf1*, *Pparg*, *Litaf*, *Nupr1*, *Rxrg*, *E2f2*, and *Zfp42* may be involved in the transcriptional regulation by 17α-estradiol in O.T (**Figure 7D**). Importantly, the activities of androgen and estrogen pathways were decreased in *Gnrh1* neurons in O.T compared to O, and were distinct from those in *Ar*, *Esr1*, and *Esr2* neurons (**Figure 7E**). These signaling pathways are important for the feedback control of sex hormone secretion in *Gnrh* neurons, and these results may also reflect the strong effect of 17α-estradiol on *Gnrh* neurons.

To decipher the potential effects of elevated serum Gnrh levels on endocrine system, we performed bidirectional MR analysis of the GWAS summary data of human GNRH1 (id: prot-a-1233) and 203 endocrine-related factors with genetic variants SNPs. We found strong causal effects of GNRH1 on GAL/Galanin (id:prot−a−1166), POMC/Beta−endorphin (id:prot−a−2327, id:prot−a−2325), Adrenomedullin (id:prot−a−48), BDNF (id:prot−a−242)**,** and LPR (id:prot−a−1724), which are involved in feeding, energy homeostasis, osmotic regulation, and neuron plasticity (**Figure 7F**). Notably, CRH/Corticotropin (id:prot−a−2326), PRLH/Prolactin−releasing peptide (id:prot−a−2376), NPW/Neuropeptide W (id:prot−a−2082), Glucagon (id:prot−a−1181), Chromogranin−A (id:prot−a−538) displayed bidirectional significance, indicating close and complex causal effects between GNRH1 and these endocrine factors (**Figure 7G, Figure 7—figure supplement 2A, B**). These results also suggest that the role

of 17α-estradiol treatment in feeding, energy homeostasis, reproduction, osmotic regulation, stress response, and neuronal plasticity may be mediated, at least in part, by elevated Gnrh secretion.

Discussion

The most striking role of 17α-estradiol treatment revealed in this study showed that HPG axis was substantially improved in the levels of serum Gnrh and testosterone. The underlying molecular mechanism remains unclear; however, prior reports have indicated that 17α-estradiol can bind to ESR1 [9]. In our findings, 17α-estradiol treatment significantly decreased serum estradiol levels while elevating serum testosterone. Based on this evidence, we propose that 17α-estradiol may function similarly to estrogen receptor antagonists or aromatase inhibitors, potentially preventing the conversion of androgens to estrogens [29, 30]. These actions could alleviate the feedback inhibition exerted by estrogen on hypothalamus and pituitary, thereby facilitating the secretion of Gnrh, FSH, and LH [31].

The testosterone levels in men gradually decline beginning in the third decade of life [32]. Age-related deterioration of the gonadotropic axis, particularly in older males with low serum testosterone, is often linked to numerous aging symptoms, including loss of skeletal muscle mass, reduced muscle strength and power, low bone mineral density, frailty, impaired physical performance, mobility limitations, increased risk of diabetes, elevated all-cause cardiovascular mortality, cognitive decline, and heightened risk of Alzheimer's disease [33]. Consequently, testosterone supplementation in older men is beneficial. Additionally, Gnrh supplementation may help mitigate age-related declines in neurogenesis and slow aging processes [34]. Importantly, treatment with 17α-estradiol did not result in feminization or adversely affect the sperm parameters and fertility in male animals [6, 14]. Thus, the observed increases in Gnrh and serum testosterone levels due to 17α-estradiol treatment are likely advantageous for older males, particularly those experiencing late-onset hypogonadism.

Postmenopausal women with low estrogen experience aging-related syndromes similar to those of older males with low serum testosterone. Those women also face increased mortality, cardiovascular disease, osteoporosis fracture, urogenital atrophy, and dementia, all of which may benefit from hormone therapy [35]. However, a prior report indicates that 17α-estradiol treatment does not provide positive life extension effects in aged females [13]. The discrepancy may stem

from the inhibitory effects of estrogens associated with 17α-estradiol treatment, as evidenced by its inability to enhance female fertility [36]. Nonetheless, due to the lack of parallel data in aged female BN rats treated with 17α-estradiol, further research is needed to definitely address this question in the female subjects in the future.

The stressed phenotype observed in neuronal subtypes discussed herein likely represents a transcriptomic manifestation of heightened physiological activity. For instance, as evidenced in this study, prolonged 17α-estradiol treatment induces a pronounced stressed phenotype in *Gnrh* neurons alongside elevated Gnrh secretion and consequent high serum testosterone levels. Similarly, the stressed phenotype reflected in the *Crh* neuronal transcriptome coincides with substantially increased serum cortisol. Furthermore, long-term 17α-estradiol treatment markedly alleviates the stressed phenotype in appetite-stimulating neurons (*Agrp* and *Ghrl*), suggesting an appetite-suppressing effect in rats. This aligns with previously reported findings that 17α-estradiol treatment inhibits feeding behavior in mice [12].

Another notable effect of 17α-estradiol is its ability to reduce the overall expression levels of energy metabolism in hypothalamic neurons of aged male BN rats. The nutrient-sensing network, mediated by MTORC1 complex, is a central regulator of mRNA and ribosome biogenesis, protein synthesis, glucose metabolism, autophagy, lipid metabolism, mitochondrial biosynthesis, and proteasomal activity [37]. Downregulation of this nutrient-sensing network has been associated with increased lifespan and healthspan [38]. Notably, 17α-estradiol treatment diminished nutrient-sensing network activity in most hypothalamic neurons, which may be a contributing factor in promoting lifespan extension.

In this report, we demonstrated significant changes in neuron populations involved in appetite control, including *Agrp*, *Pomc*, *Oxt*, *Oxtr*, *Gipr*, and *Glp2r* neurons. Among the identified subtypes, the proportion of Oxt neurons saw the most considerable increase due to 17α-estradiol treatment (**Figure 6A**). Oxt plays versatile roles in social behavior, stress response, satiety, energy balance, reproduction, and inflammation [39]. Most *Oxt* neurons originate from the paraventricular nucleus (PVN) and supraoptic nuclei (SON) in the hypothalamus, exhibiting high plasticity during development and intricate circuitry [40, 41]. The PVN, arcuate nucleus (ARC), and ventromedial hypothalamic nucleus together form a neural hub in the hypothalamus that integrates peripheral, nutritional, and metabolic signals to regulate food intake and energy balance [42]. Many effects of

Oxt are sex-specific [43]; for instance, females are less sensitive to exogenous Oxt than males regarding social recognition [44]. Interestingly, Oxt injections, facilitated by nanoparticles that enhance blood-brain barrier penetration, reduced body mass while increasing social investigation and the number of Oxt-positive cells in the SON, particularly in male rats [45]. Additionally, intracerebroventricular injections of Oxt in rats showed a reduction in food intake in both sexes, with a more pronounced effect in males [46].Therefore, we propose that Oxt's role in systemic aging and feeding behavior may contribute to the sex-biased effects of 17α-estradiol, warranting further verification.

Furthermore, 17α-estradiol treatment appears to have enhanced stress in HPA axis. One evidence was the increased levels of ferroptosis-signature and UPR in *Crh* neurons. The other evidence was the elevated serum cortisol, which is also a potential hallmark of aging HPA axis [47, 48]. Therefore, more attentions should be paid to the potential side effects of 17α-estradiol especially in its clinical application.

In summary, our findings suggest that 17α-estradiol treatment positively influences the HPG axis and neurons associated with appetite and energy balance. This may be closely linked to the life-extension effects of 17α-estradiol in aged males. Additionally, employing supervised clustering based on neuropeptides, hormones, and their receptors proves to be a valuable strategy for examining pharmacological, pathological, and physiological processes in different neuronal subtypes within the hypothalamus.

Abbreviations

Ar: androgen receptor; Agrp, agouti related neuropeptide; ARC: arcuate nucleus; Astro: astrocyte; AUC: area under the curve; Cga: glycoprotein hormones, alpha polypeptide; Crh: corticotropin releasing hormone; DEG: differentially-expressed gene; Endo: endothelial cell; Esr1: estrogen receptor 1; Esr2: estrogen receptor 2; Fibro: fibroblast; Ghrl, Ghrelin; Glp2r: glucagon-like peptide 2 receptor; GnRH: gonadotropin releasing hormone; GSEA: gene set enrichment analysis; HPA: hypothalamic–pituitary–adrenal**;** HPG: hypothalamic-pituitary-gonadal; IEU: MRC Integrative Epidemiology Unit; IVW: inverse-variance weighting; KEGG: Kyoto Encyclopedia of Genes and Genomes; Kiss1, kisspeptin, Micro: microglia; MR: Mendelian randomization; MTORC1: mechanistic target of rapamycin kinase 1; Oligo: oligodendrocyte; OPC:

oligodendrocyte precursor cell; OR: odds ratio; OXPHOS: oxidative phosphorylation; PID: Pathway Interaction Database; POMC: proopiomelanocortin; pQTL: protein quantitative trait loci; Prlh, prolactin releasing hormone; PTC: pars tuberalis cell; PVN: paraventricular nucleus; ROC: receiver operating characteristics; snRNA-seq: single-nucleus transcriptomic sequencing; Tany: tanycyte; TF: transcription factor; UPR: unfolded protein response.

Acknowledgments

We appreciate Dr. Qinghua Wang and Hongyun Shi from animal facility of Nantong University in helping with the animal experiments. Special thanks to Professor Ken-ichiro Fukuchi from University of Illinois College of Medicine for constructive comments and suggestions in manuscript preparation.

Funding: This work was supported by the National Natural Science Foundation of China grant 31271448 (YL), 82171621 (LL), 82172566 (ZY), 82150107 (RL) and the National High Level Hospital Clinical Research Funding (2022-PUMCH-A-231) (LL).

Author contributions: Conceptualization, YL, LL; Methodology, YL, GW, XX; Animal operation: YL, LL; EIA assays: YL, LY; Inflammation test: YL, ZY, LL, YS. Validation, LL, JY, ZY; Formal Analysis, YL, JY; Resources, GW, YS, ZY, ZM, LX; Visualization, YL; Writing – Original Draft, YL, JY; Writing – Review & Editing, LL, YS; Supervision, YS, ZY, YL; Project Administration, YL, ZY, LL; Funding Acquisition, ZY, LL. All authors have read and approved the final manuscript.

Declaration of competing interest

The authors have no conflict of interests to declare.

Availability of data and materials: All data are available at GEO accession number GSE248413.

Competing interests

All authors declare no competing interests.

References

1. Hajdarovic, K. H.; Yu, D.; Webb, A. E., Understanding the aging hypothalamus, one cell at a time. *Trends Neurosci* **2022,** 45, (12), 942-954.

2. Dacks, P. A.; Moreno, C. L.; Kim, E. S.; Marcellino, B. K.; Mobbs, C. V., Role of the

hypothalamus in mediating protective effects of dietary restriction during aging. *Front Neuroendocrinol* **2013,** 34, (2), 95-106.

3. Masliukov, P. M., Changes of Signaling Pathways in Hypothalamic Neurons with Aging. *Curr Issues Mol Biol* **2023,** 45, (10), 8289-8308.

4. Yang, S. B.; Tien, A. C.; Boddupalli, G.; Xu, A. W.; Jan, Y. N.; Jan, L. Y., Rapamycin ameliorates age-dependent obesity associated with increased mTOR signaling in hypothalamic POMC neurons. *Neuron* **2012,** 75, (3), 425-36.

5. Yang, H.; Fang, B.; Wang, Z.; Chen, Y.; Dong, Y., The Timing Sequence and Mechanism of Aging in Endocrine Organs. *Cells* **2023,** 12, (7).

6. Stout, M. B.; Steyn, F. J.; Jurczak, M. J.; Camporez, J. G.; Zhu, Y.; Hawse, J. R.; Jurk, D.; Palmer, A. K.; Xu, M.; Pirtskhalava, T.; Evans, G. L.; de Souza Santos, R.; Frank, A. P.; White, T. A.; Monroe, D. G.; Singh, R. J.; Casaclang-Verzosa, G.; Miller, J. D.; Clegg, D. J.; LeBrasseur, N. K.; von Zglinicki, T.; Shulman, G. I.; Tchkonia, T.; Kirkland, J. L., 17α-Estradiol Alleviates Age-related Metabolic and Inflammatory Dysfunction in Male Mice Without Inducing Feminization. *J Gerontol A Biol Sci Med Sci* **2017,** 72, (1), 3-15.

7. Shen, Z.; Hinson, A.; Miller, R. A.; Garcia, G. G., Cap-independent translation: A shared mechanism for lifespan extension by rapamycin, acarbose, and 17α-estradiol. *Aging Cell* **2021,** 20, (5), e13345.

8. Wink, L.; Miller, R. A.; Garcia, G. G., Rapamycin, Acarbose and 17α-estradiol share common mechanisms regulating the MAPK pathways involved in intracellular signaling and inflammation. *Immun Ageing* **2022,** 19, (1), 8.

9. Mann, S. N.; Hadad, N.; Nelson Holte, M.; Rothman, A. R.; Sathiaseelan, R.; Ali Mondal, S.; Agbaga, M. P.; Unnikrishnan, A.; Subramaniam, M.; Hawse, J.; Huffman, D. M.; Freeman, W. M.; Stout, M. B., Health benefits attributed to 17α-estradiol, a lifespan-extending compound, are mediated through estrogen receptor α. *Elife* **2020,** 9.

10. Watanabe, K.; Wilmanski, T.; Baloni, P.; Robinson, M.; Garcia, G. G.; Hoopmann, M. R.; Midha, M. K.; Baxter, D. H.; Maes, M.; Morrone, S. R.; Crebs, K. M.; Kapil, C.; Kusebauch, U.; Wiedrick, J.; Lapidus, J.; Pflieger, L.; Lausted, C.; Roach, J. C.; Glusman, G.; Cummings, S. R.; Schork, N. J.; Price, N. D.; Hood, L.; Miller, R. A.; Moritz, R. L.; Rappaport, N., Lifespan-extending interventions induce consistent patterns of fatty acid oxidation in mouse livers. *Commun Biol* **2023,** 6, (1), 768.

11. Burns, A. R.; Wiedrick, J.; Feryn, A.; Maes, M.; Midha, M. K.; Baxter, D. H.; Morrone, S. R.; Prokop, T. J.; Kapil, C.; Hoopmann, M. R.; Kusebauch, U.; Deutsch, E. W.; Rappaport, N.; Watanabe, K.; Moritz, R. L.; Miller, R. A.; Lapidus, J. A.; Orwoll, E. S., Proteomic changes induced by longevity-promoting interventions in mice. *Geroscience* **2024,** 46, (2), 1543-1560.

12. Steyn, F. J.; Ngo, S. T.; Chen, V. P.; Bailey-Downs, L. C.; Xie, T. Y.; Ghadami, M.; Brimijoin, S.; Freeman, W. M.; Rubinstein, M.; Low, M. J.; Stout, M. B., 17α-estradiol acts through hypothalamic pro-opiomelanocortin expressing neurons to reduce feeding behavior. *Aging Cell* **2018,** 17, (1).

13. Harrison, D. E.; Strong, R.; Allison, D. B.; Ames, B. N.; Astle, C. M.; Atamna, H.; Fernandez, E.; Flurkey, K.; Javors, M. A.; Nadon, N. L.; Nelson, J. F.; Pletcher, S.;

Simpkins, J. W.; Smith, D.; Wilkinson, J. E.; Miller, R. A., Acarbose, 17-α-estradiol, and nordihydroguaiaretic acid extend mouse lifespan preferentially in males. *Aging Cell* **2014,** 13, (2), 273-82.

14. Isola, J. V. V.; Veiga, G. B.; de Brito, C. R. C.; Alvarado-Rincón, J. A.; Garcia, D. N.; Zanini, B. M.; Hense, J. D.; Vieira, A. D.; Garratt, M.; Gasperin, B. G.; Schneider, A.; Stout, M. B., 17α-estradiol does not adversely affect sperm parameters or fertility in male mice: implications for reproduction-longevity trade-offs. *Geroscience* **2023,** 45, (4), 2109-2120.

15. Stout, M. B.; Vaughan, K. L.; Isola, J. V. V.; Mann, S. N.; Wellman, B.; Hoffman, J. M.; Porter, H. L.; Freeman, W. M.; Mattison, J. A., Assessing tolerability and physiological responses to 17α-estradiol administration in male rhesus macaques. *Geroscience* **2023,** 45, (4), 2337-2349.

16. Harrison, D. E.; Strong, R.; Reifsnyder, P.; Kumar, N.; Fernandez, E.; Flurkey, K.; Javors, M. A.; Lopez-Cruzan, M.; Macchiarini, F.; Nelson, J. F.; Markewych, A.; Bitto, A.; Sindler, A. L.; Cortopassi, G.; Kavanagh, K.; Leng, L.; Bucala, R.; Rosenthal, N.; Salmon, A.; Stearns, T. M.; Bogue, M.; Miller, R. A., 17-a-estradiol late in life extends lifespan in aging UM-HET3 male mice; nicotinamide riboside and three other drugs do not affect lifespan in either sex. *Aging Cell* **2021,** 20, (5), e13328.

17. Strong, R.; Miller, R. A.; Antebi, A.; Astle, C. M.; Bogue, M.; Denzel, M. S.; Fernandez, E.; Flurkey, K.; Hamilton, K. L.; Lamming, D. W.; Javors, M. A.; de Magalhães, J. P.; Martinez, P. A.; McCord, J. M.; Miller, B. F.; Müller, M.; Nelson, J. F.; Ndukum, J.; Rainger, G. E.; Richardson, A.; Sabatini, D. M.; Salmon, A. B.; Simpkins, J. W.;

Steegenga, W. T.; Nadon, N. L.; Harrison, D. E., Longer lifespan in male mice treated with a weakly estrogenic agonist, an antioxidant, an α-glucosidase inhibitor or a Nrf2-inducer. *Aging Cell* **2016,** 15, (5), 872-84.

18. Rath, S.; Sharma, R.; Gupta, R.; Ast, T.; Chan, C.; Durham, T. J.; Goodman, R. P.; Grabarek, Z.; Haas, M. E.; Hung, W. H. W.; Joshi, P. R.; Jourdain, A. A.; Kim, S. H.; Kotrys, A. V.; Lam, S. S.; McCoy, J. G.; Meisel, J. D.; Miranda, M.; Panda, A.; Patgiri, A.; Rogers, R.; Sadre, S.; Shah, H.; Skinner, O. S.; To, T. L.; Walker, M. A.; Wang, H.; Ward, P. S.; Wengrod, J.; Yuan, C. C.; Calvo, S. E.; Mootha, V. K., MitoCarta3.0: an updated mitochondrial proteome now with sub-organelle localization and pathway annotations. *Nucleic Acids Res* **2021,** 49, (D1), D1541-d1547.

19. Hu, H.; Miao, Y. R.; Jia, L. H.; Yu, Q. Y.; Zhang, Q.; Guo, A. Y., AnimalTFDB 3.0: a comprehensive resource for annotation and prediction of animal transcription factors. *Nucleic Acids Res* **2019,** 47, (D1), D33-d38.

20. Lu, H.; Ping, J.; Zhou, G.; Zhao, Z.; Gao, W.; Jiang, Y.; Quan, C.; Lu, Y.; Zhou, G., CommPath: An R package for inference and analysis of pathway-mediated cell-cell communication chain from single-cell transcriptomics. *Comput Struct Biotechnol J* **2022,** 20, 5978-5983.

21. Badia, I. M. P.; Vélez Santiago, J.; Braunger, J.; Geiss, C.; Dimitrov, D.; Müller-Dott, S.; Taus, P.; Dugourd, A.; Holland, C. H.; Ramirez Flores, R. O.; Saez-Rodriguez, J., decoupleR: ensemble of computational methods to infer biological activities from omics data. *Bioinform Adv* **2022,** 2, (1), vbac016.

22. Skinnider, M. A.; Squair, J. W.; Kathe, C.; Anderson, M. A.; Gautier, M.; Matson, K. J.

E.; Milano, M.; Hutson, T. H.; Barraud, Q.; Phillips, A. A.; Foster, L. J.; La Manno, G.; Levine, A. J.; Courtine, G., Cell type prioritization in single-cell data. *Nat Biotechnol* **2021,** 39, (1), 30-34.

23. Liao, Y.; Wang, J.; Jaehnig, E. J.; Shi, Z.; Zhang, B., WebGestalt 2019: gene set analysis toolkit with revamped UIs and APIs. *Nucleic Acids Res* **2019,** 47, (W1), W199-w205.

24. Hemani, G.; Zheng, J.; Elsworth, B.; Wade, K. H.; Haberland, V.; Baird, D.; Laurin, C.; Burgess, S.; Bowden, J.; Langdon, R.; Tan, V. Y.; Yarmolinsky, J.; Shihab, H. A.; Timpson, N. J.; Evans, D. M.; Relton, C.; Martin, R. M.; Davey Smith, G.; Gaunt, T. R.; Haycock, P. C., The MR-Base platform supports systematic causal inference across the human phenome. *Elife* **2018,** 7.

25. Sun, B. B.; Maranville, J. C.; Peters, J. E.; Stacey, D.; Staley, J. R.; Blackshaw, J.; Burgess, S.; Jiang, T.; Paige, E.; Surendran, P.; Oliver-Williams, C.; Kamat, M. A.; Prins, B. P.; Wilcox, S. K.; Zimmerman, E. S.; Chi, A.; Bansal, N.; Spain, S. L.; Wood, A. M.; Morrell, N. W.; Bradley, J. R.; Janjic, N.; Roberts, D. J.; Ouwehand, W. H.; Todd, J. A.; Soranzo, N.; Suhre, K.; Paul, D. S.; Fox, C. S.; Plenge, R. M.; Danesh, J.; Runz, H.; Butterworth, A. S., Genomic atlas of the human plasma proteome. *Nature* **2018,** 558, (7708), 73-79.

26. Hemani, G.; Tilling, K.; Davey Smith, G., Orienting the causal relationship between imprecisely measured traits using GWAS summary data. *PLoS Genet* **2017,** 13, (11), e1007081.

27. Inada, K.; Tsujimoto, K.; Yoshida, M.; Nishimori, K.; Miyamichi, K., Oxytocin signaling

in the posterior hypothalamus prevents hyperphagic obesity in mice. *Elife* **2022,** 11.

28. Dalvi, P. S.; Belsham, D. D., Glucagon-like peptide-2 directly regulates hypothalamic neurons expressing neuropeptides linked to appetite control in vivo and in vitro. *Endocrinology* **2012,** 153, (5), 2385-97.

29. Leder, B. Z.; Rohrer, J. L.; Rubin, S. D.; Gallo, J.; Longcope, C., Effects of aromatase inhibition in elderly men with low or borderline-low serum testosterone levels. *J Clin Endocrinol Metab* **2004,** 89, (3), 1174-80.

30. Guay, A. T.; Jacobson, J.; Perez, J. B.; Hodge, M. B.; Velasquez, E., Clomiphene increases free testosterone levels in men with both secondary hypogonadism and erectile dysfunction: who does and does not benefit? *Int J Impot Res* **2003,** 15, (3), 156-65.

31. Wang, C.; Swerdloff, R. S., Testosterone Replacement Therapy in Hypogonadal Men. *Endocrinol Metab Clin North Am* **2022,** 51, (1), 77-98.

32. Camacho, E. M.; Huhtaniemi, I. T.; O'Neill, T. W.; Finn, J. D.; Pye, S. R.; Lee, D. M.; Tajar, A.; Bartfai, G.; Boonen, S.; Casanueva, F. F.; Forti, G.; Giwercman, A.; Han, T. S.; Kula, K.; Keevil, B.; Lean, M. E.; Pendleton, N.; Punab, M.; Vanderschueren, D.; Wu, F. C., Age-associated changes in hypothalamic-pituitary-testicular function in middle-aged and older men are modified by weight change and lifestyle factors: longitudinal results from the European Male Ageing Study. *Eur J Endocrinol* **2013,** 168, (3), 445-55.

33. Rodrigues Dos Santos, M.; Bhasin, S., Benefits and Risks of Testosterone Treatment in Men with Age-Related Decline in Testosterone. *Annu Rev Med* **2021,** 72, 75-91.

34. Zhang, G.; Li, J.; Purkayastha, S.; Tang, Y.; Zhang, H.; Yin, Y.; Li, B.; Liu, G.; Cai, D., Hypothalamic programming of systemic ageing involving IKK-β, NF-κB and GnRH. *Nature* **2013,** 497, (7448), 211-6.

35. Shoupe, D., Individualizing hormone therapy to minimize risk: accurate assessment of risks and benefits. *Womens Health (Lond)* **2011,** 7, (4), 475-85.

36. Isola, J. V. V.; Zanini, B. M.; Hense, J. D.; Alvarado-Rincón, J. A.; Garcia, D. N.; Pereira, G. C.; Vieira, A. D.; Oliveira, T. L.; Collares, T.; Gasperin, B. G.; Stout, M. B.; Schneider, A., Mild calorie restriction, but not 17α-estradiol, extends ovarian reserve and fertility in female mice. *Exp Gerontol* **2022,** 159, 111669.

37. López-Otín, C.; Blasco, M. A.; Partridge, L.; Serrano, M.; Kroemer, G., Hallmarks of aging: An expanding universe. *Cell* **2023,** 186, (2), 243-278.

38. Singh, P. P.; Demmitt, B. A.; Nath, R. D.; Brunet, A., The Genetics of Aging: A Vertebrate Perspective. *Cell* **2019,** 177, (1), 200-220.

39. Kerem, L.; Lawson, E. A., The Effects of Oxytocin on Appetite Regulation, Food Intake and Metabolism in Humans. *Int J Mol Sci* **2021,** 22, (14).

40. Rosen, G. J.; de Vries, G. J.; Goldman, S. L.; Goldman, B. D.; Forger, N. G., Distribution of oxytocin in the brain of a eusocial rodent. *Neuroscience* **2008,** 155, (3), 809-17.

41. Madrigal, M. P.; Jurado, S., Specification of oxytocinergic and vasopressinergic circuits in the developing mouse brain. *Commun Biol* **2021,** 4, (1), 586.

42. Cornejo, M. P.; Hentges, S. T.; Maliqueo, M.; Coirini, H.; Becu-Villalobos, D.; Elias, C. F., Neuroendocrine Regulation of Metabolism. *J Neuroendocrinol* **2016,** 28, (7).

753 43. Carvalho Silva, R.; Pisanu, C.; Maffioletti, E.; Menesello, V.; Bortolomasi, M.;
754 Gennarelli, M.; Baune, B. T.; Squassina, A.; Minelli, A., Biological markers of
755 sex-based differences in major depressive disorder and in antidepressant response.
756 *Eur Neuropsychopharmacol* **2023,** 76, 89-107.
757 44. Dumais, K. M.; Veenema, A. H., Vasopressin and oxytocin receptor systems in the
758 brain: Sex differences and sex-specific regulation of social behavior. *Front*
759 *Neuroendocrinol* **2016,** 40, 1-23.
760 45. Duarte-Guterman, P.; Lieblich, S. E.; Qiu, W.; Splinter, J. E. J.; Go, K. A.;
761 Casanueva-Reimon, L.; Galea, L. A. M., Oxytocin has sex-specific effects on social
762 behaviour and hypothalamic oxytocin immunoreactive cells but not hippocampal
763 neurogenesis in adult rats. *Horm Behav* **2020,** 122, 104734.
764 46. Liu, C. M.; Davis, E. A.; Suarez, A. N.; Wood, R. I.; Noble, E. E.; Kanoski, S. E., Sex
765 Differences and Estrous Influences on Oxytocin Control of Food Intake. *Neuroscience*
766 **2020,** 447, 63-73.
767 47. Veldhuis, J. D., Changes in pituitary function with ageing and implications for patient
768 care. *Nat Rev Endocrinol* **2013,** 9, (4), 205-15.
769 48. Warde, K. M.; Smith, L. J.; Basham, K. J., Age-related Changes in the Adrenal Cortex:
770 Insights and Implications. *J Endocr Soc* **2023,** 7, (9), bvad097.

771

772 **Figure legends**

773 **Figure 1. snRNA-seq profiling of the hypothalamus from O, O.T and Y samples. (A)** UMAP
774 visualization of nuclei colored by 10 cell types: neuron (Neu), astrocyte (Astro), oligodendrocyte
775 (Oligo), oligodendrocyte precursor cell (OPC), tanycyte (Tany), ependymocyte (Epen), microglia
776 (Micro), fibroblast (Fibro), pars tuberalis cell (PTC), and endothelial cell (Endo), from

777 hypothalamus of aged rats (O), 17α-estradiol-treated aged rats (O.T) and young rats (Y). **(B)**
778 Heatmap showing the classic markers of 10 major cell types in hypothalamus. **(C)** Cell-type
779 compositions by groups (left panel) or by major cell types with the total cell numbers shown
780 above each column. **(D)** Circos plot depicting the number of ligand–receptor pairs between Neu
781 and other cell types (color strips) for each group. **(E)** Dot plot showing significant ligand–receptor
782 interactions between Neurons for each group. Boxes showing the unique ligand–receptor
783 interactions between Neuron.O (black boxes) or between Neuron.O.T (blue boxes). **(F)** Dot plot of
784 the top 6 enriched GO biological process terms across three groups of neurons via GSEA analysis.
785 **(G)** The top 15 changed pathways/gene sets according to the ranks of AUC values in selected
786 pathways related to neuronal synapses and axons from Gene Ontology (GO) biological process,
787 GO molecular function and GO cellular component.
788
789 **Figure 2. Two opposing regulatory signaling networks in neuron metabolism. (A)** Dot plot of
790 the selected pathways representing the prominent changes of overall expression levels across
791 Neuron.O, Neuron.O.T and Neuron.Y in metabolism, signaling and synaptic activity. **(B)**
792 Correlation heatmap showing transcription factors (TFs) that correlated with the two opposing
793 regulatory signaling networks in the mixed neurons of O, O.T and Y. **(C)** The shared unique
794 markers of each quarter (c1-c4) in 6 pathways in hypothalamic neurons (O, O.T, and Y). The
795 markers were then collected as c1.up.signature (19 genes) and c4.up.signature (12 genes). **(D)** The
796 aging-related cell proportions of each quarter shown by 4 pathways. **(E)** The correlation of
797 c1.up.signature and c2.up.signature with the two opposing regulatory signaling networks.
798
799 **Figure 3. Screening of neuron subtypes via supervised clustering, which responded distinctly**
800 **to aging and 17α-estradiol treatment. (A)** Diagram outlining the features of supervised
801 clustering of neurons in the hypothalamus in comparison with traditional unsupervised clustering.
802 **(B)** The ranks of cell counts in neuropeptide-secreting neuron subclusters (left panel) and
803 subclusters expressing neuropeptide receptors or hormone receptors (right panel) in sample Y. The
804 cell number (n) in each subset is ≥ 10. **(C, D)** The prioritization of the top 20 neuron subclusters
805 across the 3 types of perturbation (O vs Y, O.T vs Y, and O.T vs O) calculated by the Augur
806 algorithm, in neuropeptide-secreting neurons (C) and neuron subclusters expressing neuropeptide

807 receptors or hormone receptors (D).

808

809 **Figure 4. Ranking of neuron subtypes with distinct responses to aging and 17α-estradiol**
810 **treatment. (A, B)** The top 20 and bottom 20 neuron subtypes based on the mean expression
811 values of five signatures or gene sets, ranked by their values in sample O, in
812 neuropeptide-secreting subtypes (A) and in neuron subtypes expressing neuropeptide receptors or
813 hormone receptors (B).

814

815 **Figure 5. Responses of Crh neurons to long-term 17α-estradiol treatment. (A)** The top 20 and
816 bottom 20 neuropeptide-secreting neuron subtypes, ranked by their mean expression values of five
817 signatures or gene sets in sample O. **(B)** Expression profiles of selected pathways from two
818 opposing signaling networks in *Crh*, *Kiss1*, and *Prlh* neurons. **(C)** Downregulated and upregulated
819 differentially expressed genes (DEGs) associated with mitochondria or the adherens junction
820 pathway in *Crh* neurons, comparing O.T vs O. **(D)** Top 25 transcription factor (TF) activities in
821 *Crh* and *Gnrh1* neurons. **(E)** Serum levels of Crh, cortisol, and aldosterone in Y, O, and O.T
822 groups as measured by enzyme immunoassay; two-tailed unpaired t-tests were performed, with
823 p-values indicated.

824

825 **Figure 6. The response of *Oxt* neurons to 17α-estradiol and the causal effects of Oxt on other**
826 **endocrine factors.**
827 **(A)** The relative cell proportions of peptide-expressing subclusters (upper panel) and
828 receptor-expressing subclusters (lower panel) across Y, O, and O.T (sorted in descending order of
829 proportions in Y). Only subclusters with a cell count of $n \geq 10$ in sample Y were included for
830 calculation. **(B)** Dot plots showing the expression profiles of the selected pathways from the two
831 opposing signaling pathways in four types of food uptake-related neurons, which decreased or
832 increased among the top 10 ranks in (A) or (B). Blue arrows: c1.up.signature and c4.up.signature.
833 **(C)** Volcanic plots showing the DEGs between Neuron.O.T and Neuron.O in the pathway synaptic
834 membrane. **(D)** Enzyme immunoassay of the plasma levels of Oxt in three groups. **(E)** Top 25 TF
835 activities in neuron Oxt. **(F)** Significant causal effects ($p < 0.05$, IVW) between exposure OXT (id:
836 prot-a-2159) and 203 endocrine-related outcomes, which were not significant in reverse MR

837 analysis. Significant heterogeneity (Q_pval < 0.05). Significant horizontal pleiotropy (pval <
838 0.05).
839
840 **Figure 7. The response of HPG axis in the males to 17α-estradiol and the causal effects of**
841 **Gnrh on other endocrine factors. (A)** The expression profiles of pathways from the two
842 opposing signaling networks in *Gnrh1*-, *Esr2*-, *Esr1*- or *Ar*-positive neurons. **(B)** Enzyme
843 immunoassay of the serum levels of Gnrh, total testosterone (T), and estrogen (E) in Y, O and O.T
844 samples. Two-tail unpaired T-test was performed. **(C)** Inflammation of seminiferous tubules in
845 testes of O and O.T. Left two panels: representative HE staining of testis inflammation in O and
846 the normal seminiferous tubules of O.T. Right panel: the mean testis inflammation index of O and
847 O.T. **(D)** The top 25 TF activities in *Gnrh1* neurons in three groups. **(E)** The activities of 14
848 pathways in *Gnrh1*-, *Esr2*-, *Esr1*- or *Ar*-positive neurons. **(F)** Significant causal effects (IVW, p <
849 0.05) between exposure GNRH1 (id: prot-a-1233) and 203 endocrine-related outcomes, which
850 were not significant in reverse MR analysis. **(G)** Items with significant causal effects (IVW, p <
851 0.05) in both directions of MR analysis between GNRH1 (id: prot-a-1233) and 203
852 endocrine-related outcomes.
853
854
855

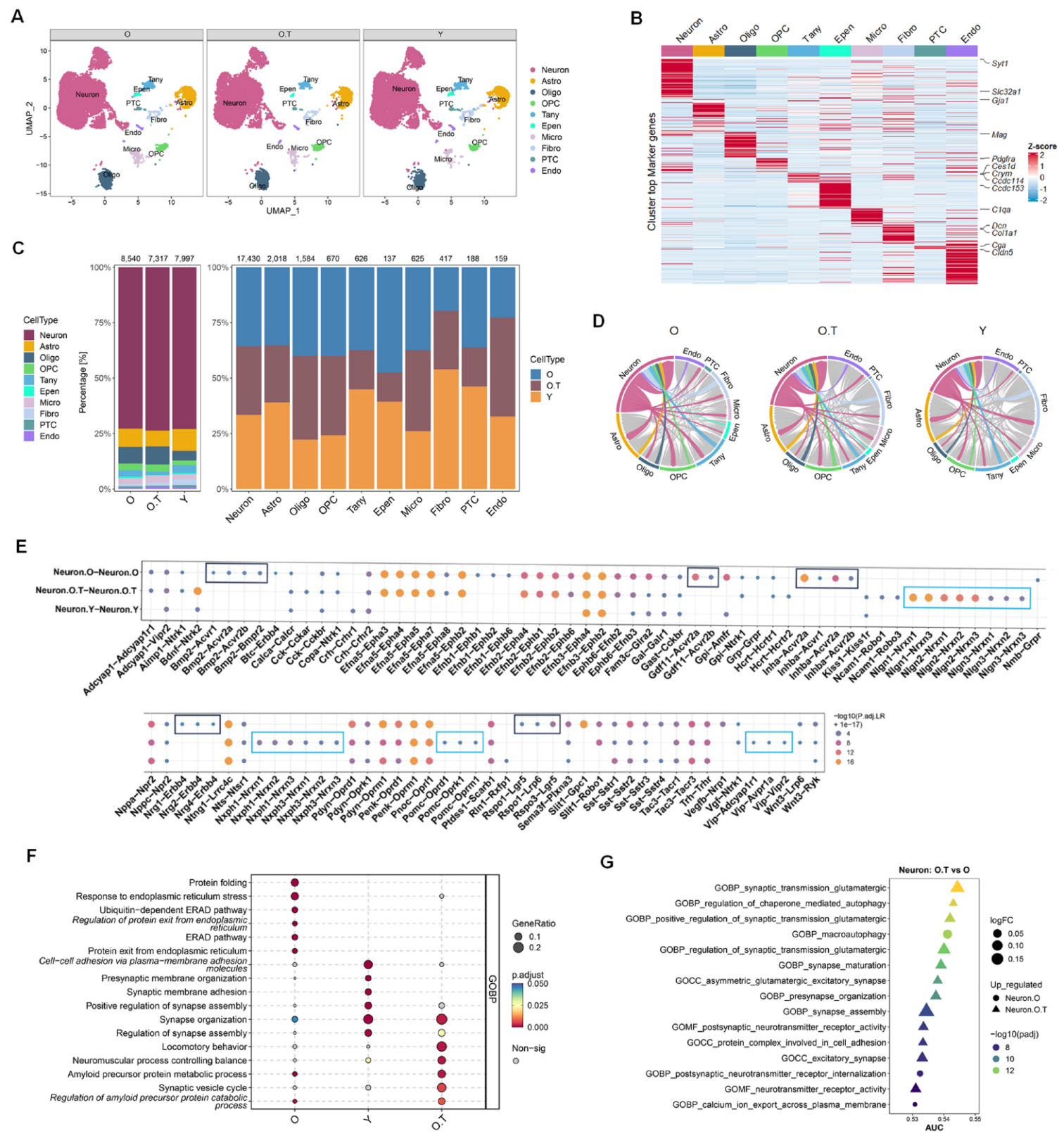
A
O
O.T
Y
UMAP_1
UMAP_2
Neuron
Astro
Oligo
OPC
Tany
Epen
Micro
Fibro
PTC
Endo
B
Cluster top Marker genes
Z-score
Syt1
Slc32a1
Gja1
Mag
Pdgfra
Ces1d
Crym
Ccdc114
Ccdc153
C1qa
Dcn
Col1a1
Cga
Cldn5
C
CellType
Percentage [%]
8,540
7,317
7,997
17,430
2,018
1,584
670
626
137
625
417
188
159
D
E
Neuron.O−Neuron.O
Neuron.O.T−Neuron.O.T
Neuron.Y−Neuron.Y
−log10(P.adj.LR + 1e−17)
F
Protein folding
Response to endoplasmic reticulum stress
Ubiquitin−dependent ERAD pathway
Regulation of protein exit from endoplasmic reticulum
ERAD pathway
Protein exit from endoplasmic reticulum
Cell−cell adhesion via plasma−membrane adhesion molecules
Presynaptic membrane organization
Synaptic membrane adhesion
Positive regulation of synapse assembly
Synapse organization
Regulation of synapse assembly
Locomotory behavior
Neuromuscular process controlling balance
Amyloid precursor protein metabolic process
Synaptic vesicle cycle
Regulation of amyloid precursor protein catabolic process
GOBP
GeneRatio
p.adjust
Non−sig
G
Neuron: O.T vs O
GOBP_synaptic_transmission_glutamatergic
GOBP_regulation_of_chaperone_mediated_autophagy
GOBP_positive_regulation_of_synaptic_transmission_glutamatergic
GOBP_macroautophagy
GOBP_regulation_of_synaptic_transmission_glutamatergic
GOBP_synapse_maturation
GOCC_asymmetric_glutamatergic_excitatory_synapse
GOBP_presynapse_organization
GOBP_synapse_assembly
GOMF_postsynaptic_neurotransmitter_receptor_activity
GOCC_protein_complex_involved_in_cell_adhesion
GOCC_excitatory_synapse
GOBP_postsynaptic_neurotransmitter_receptor_internalization
GOMF_neurotransmitter_receptor_activity
GOBP_calcium_ion_export_across_plasma_membrane
logFC
Up_regulated
−log10(padj)
AUC

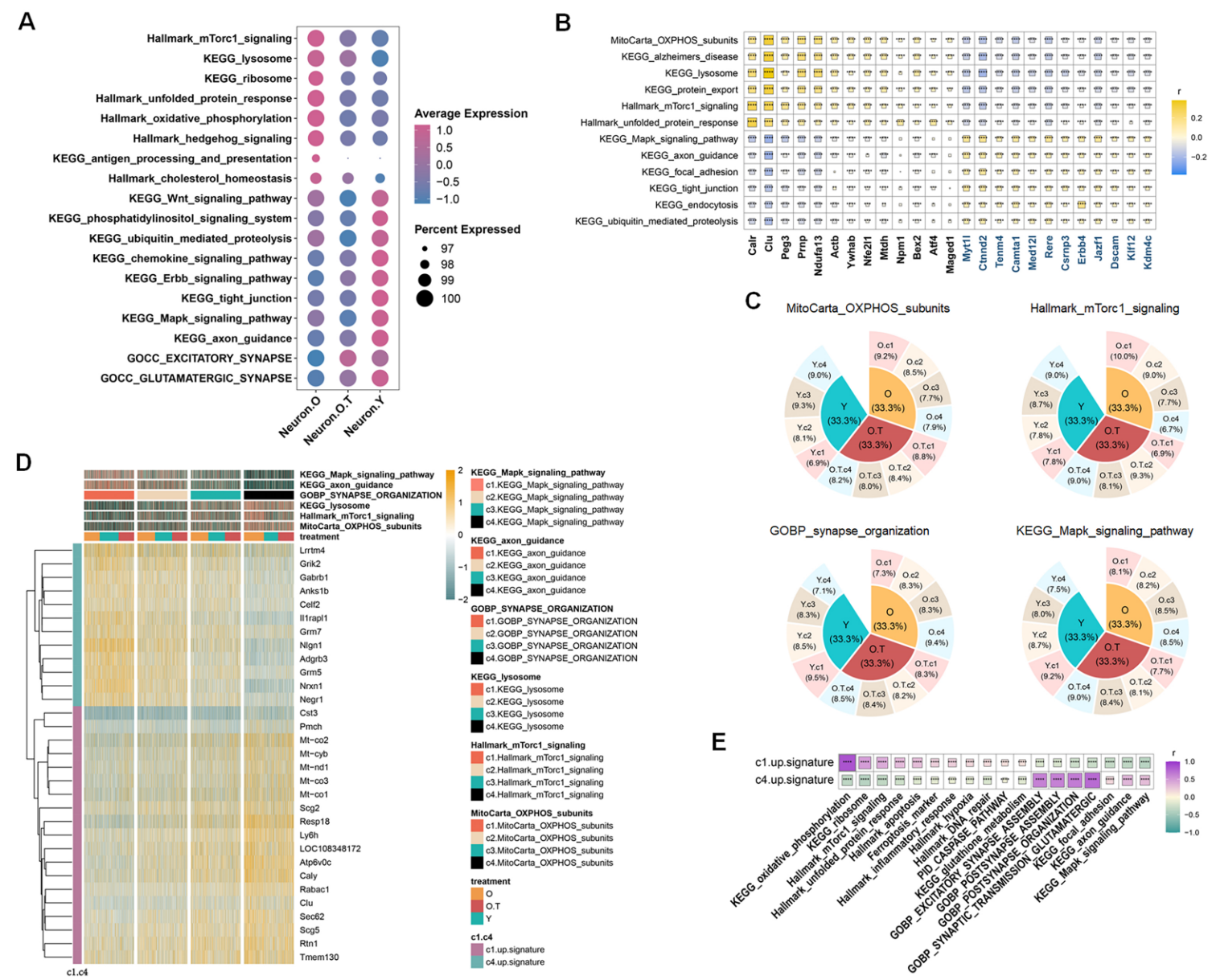
A
Hallmark_mTorc1_signaling
KEGG_lysosome
KEGG_ribosome
Hallmark_unfolded_protein_response
Hallmark_oxidative_phosphorylation
Hallmark_hedgehog_signaling
KEGG_antigen_processing_and_presentation
Hallmark_cholesterol_homeostasis
KEGG_Wnt_signaling_pathway
KEGG_phosphatidylinositol_signaling_system
KEGG_ubiquitin_mediated_proteolysis
KEGG_chemokine_signaling_pathway
KEGG_Erbb_signaling_pathway
KEGG_tight_junction
KEGG_Mapk_signaling_pathway
KEGG_axon_guidance
GOCC_EXCITATORY_SYNAPSE
GOCC_GLUTAMATERGIC_SYNAPSE
Neuron.O
Neuron.O.T
Neuron.Y
Average Expression
1.0
0.5
0.0
−0.5
−1.0
Percent Expressed
97
98
99
100
B
MitoCarta_OXPHOS_subunits
KEGG_alzheimers_disease
KEGG_lysosome
KEGG_protein_export
Hallmark_mTorc1_signaling
Hallmark_unfolded_protein_response
KEGG_Mapk_signaling_pathway
KEGG_axon_guidance
KEGG_focal_adhesion
KEGG_tight_junction
KEGG_endocytosis
KEGG_ubiquitin_mediated_proteolysis
Calr
Clu
Peg3
Pnp
Ndufa13
Actb
Ywhab
Nfe2l1
Mtdh
Npm1
Bex2
Atf4
Maged1
Myt1l
Ctnnd2
Tenm4
Camta1
Med12l
Rere
Csrnp3
Erbb4
Jazf1
Dscam
Klf12
Kdm4c
r
0.2
0.0
−0.2
C
MitoCarta_OXPHOS_subunits
Hallmark_mTorc1_signaling
GOBP_synapse_organization
KEGG_Mapk_signaling_pathway
O
O.T
Y
(33.3%)
O.c1 (9.2%)
O.c2 (8.5%)
O.c3 (7.7%)
O.c4 (7.9%)
O.T.c1 (8.8%)
O.T.c2 (8.4%)
O.T.c3 (8.0%)
O.T.c4 (8.2%)
Y.c1 (6.9%)
Y.c2 (8.1%)
Y.c3 (9.3%)
Y.c4 (9.0%)
O.c1 (10.0%)
O.c2 (9.0%)
O.c3 (7.7%)
O.c4 (6.7%)
O.T.c1 (6.9%)
O.T.c2 (9.3%)
O.T.c3 (8.1%)
O.T.c4 (9.0%)
Y.c1 (7.8%)
Y.c2 (7.8%)
Y.c3 (8.7%)
Y.c4 (9.0%)
O.c1 (7.3%)
O.c2 (8.3%)
O.c3 (8.3%)
O.c4 (9.4%)
O.T.c1 (8.3%)
O.T.c2 (8.2%)
O.T.c3 (8.4%)
O.T.c4 (8.5%)
Y.c1 (9.5%)
Y.c2 (8.5%)
Y.c3 (8.3%)
Y.c4 (7.1%)
O.c1 (8.1%)
O.c2 (8.2%)
O.c3 (8.5%)
O.c4 (8.5%)
O.T.c1 (7.7%)
O.T.c2 (8.1%)
O.T.c3 (8.4%)
O.T.c4 (9.0%)
Y.c1 (9.2%)
Y.c2 (8.7%)
Y.c3 (8.0%)
Y.c4 (7.5%)
D
KEGG_Mapk_signaling_pathway
KEGG_axon_guidance
GOBP_SYNAPSE_ORGANIZATION
KEGG_lysosome
Hallmark_mTorc1_signaling
MitoCarta_OXPHOS_subunits
treatment
Lrrtm4
Grik2
Gabrb1
Anks1b
Celf2
Il1rapl1
Grm7
Nlgn1
Adgrb3
Grm5
Nrxn1
Negr1
Cst3
Pmch
Mt−co2
Mt−cyb
Mt−nd1
Mt−co3
Mt−co1
Scg2
Resp18
Ly6h
LOC108348172
Atp6v0c
Caly
Rabac1
Clu
Sec62
Scg5
Rtn1
Tmem130
c1.c4
2
1
0
−1
−2
KEGG_Mapk_signaling_pathway
c1.KEGG_Mapk_signaling_pathway
c2.KEGG_Mapk_signaling_pathway
c3.KEGG_Mapk_signaling_pathway
c4.KEGG_Mapk_signaling_pathway
KEGG_axon_guidance
c1.KEGG_axon_guidance
c2.KEGG_axon_guidance
c3.KEGG_axon_guidance
c4.KEGG_axon_guidance
GOBP_SYNAPSE_ORGANIZATION
c1.GOBP_SYNAPSE_ORGANIZATION
c2.GOBP_SYNAPSE_ORGANIZATION
c3.GOBP_SYNAPSE_ORGANIZATION
c4.GOBP_SYNAPSE_ORGANIZATION
KEGG_lysosome
c1.KEGG_lysosome
c2.KEGG_lysosome
c3.KEGG_lysosome
c4.KEGG_lysosome
Hallmark_mTorc1_signaling
c1.Hallmark_mTorc1_signaling
c2.Hallmark_mTorc1_signaling
c3.Hallmark_mTorc1_signaling
c4.Hallmark_mTorc1_signaling
MitoCarta_OXPHOS_subunits
c1.MitoCarta_OXPHOS_subunits
c2.MitoCarta_OXPHOS_subunits
c3.MitoCarta_OXPHOS_subunits
c4.MitoCarta_OXPHOS_subunits
treatment
O
O.T
Y
c1.c4
c1.up.signature
c4.up.signature
E
c1.up.signature
c4.up.signature
KEGG_oxidative_phosphorylation
KEGG_ribosome
Hallmark_mTorc1_signaling
Hallmark_unfolded_protein_response
Hallmark_apoptosis
Ferroptosis_marker
Hallmark_inflammatory_response
Hallmark_hypoxia
Hallmark_DNA_repair
PID_CASPASE_PATHWAY
KEGG_glutathione_metabolism
GOBP_EXCITATORY_SYNAPSE_ASSEMBLY
GOBP_POSTSYNAPSE_ASSEMBLY
GOBP_POSTSYNAPSE_ORGANIZATION
GOBP_SYNAPTIC_TRANSMISSION_GLUTAMATERGIC
KEGG_focal_adhesion
KEGG_axon_guidance
KEGG_Mapk_signaling_pathway
r
1.0
0.5
0.0
−0.5
−1.0

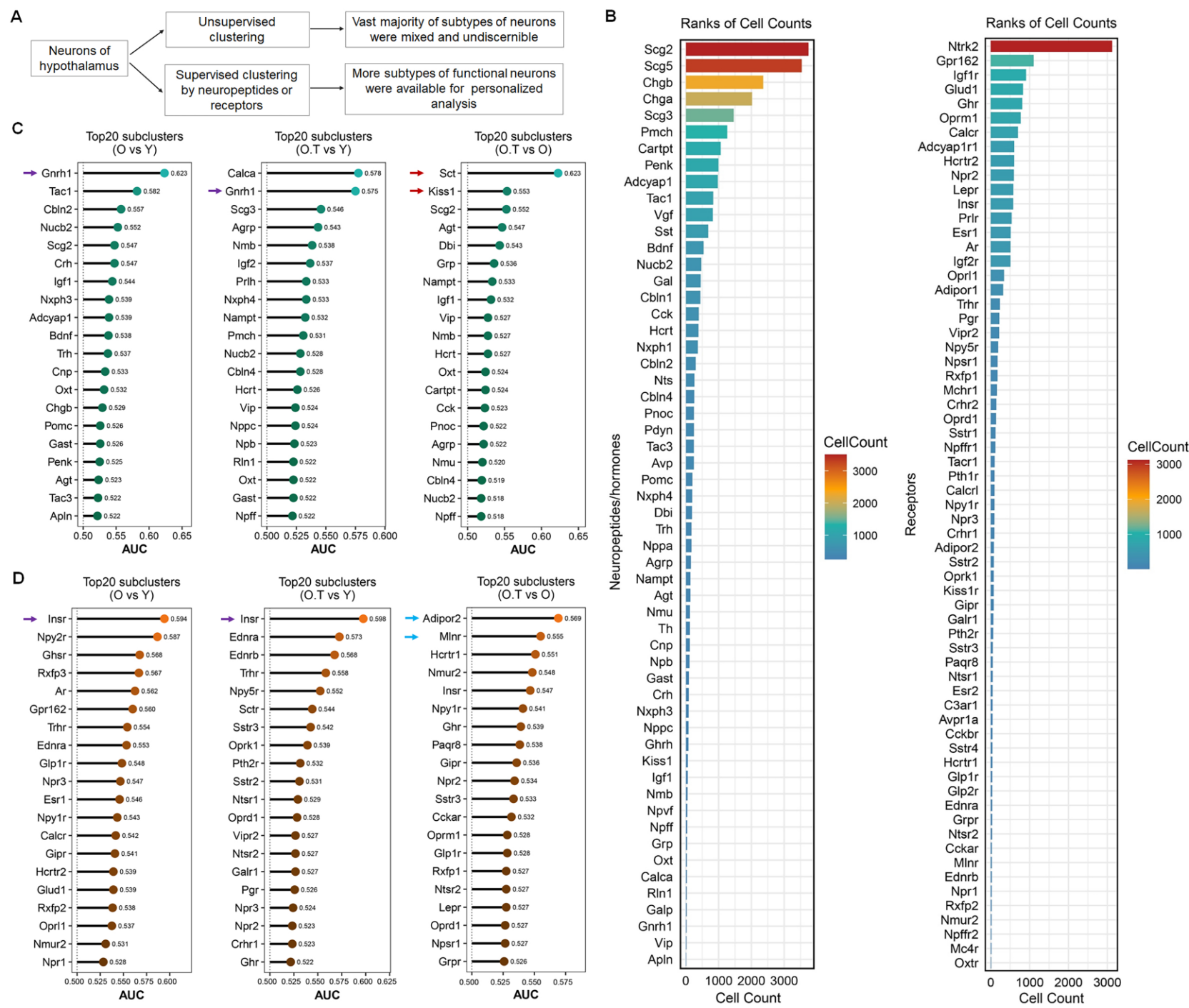
A
Neurons of hypothalamus
Unsupervised clustering
Vast majority of subtypes of neurons were mixed and undiscernible
Supervised clustering by neuropeptides or receptors
More subtypes of functional neurons were available for personalized analysis
B
Ranks of Cell Counts
Neuropeptides/hormones
Scg2 Scg5 Chgb Chga Scg3 Pmch Cartpt Penk Adcyap1 Tac1 Vgf Sst Bdnf Nucb2 Gal Cbln1 Cck Hcrt Nxph1 Cbln2 Nts Cbln4 Pnoc Pdyn Tac3 Avp Pomc Nxph4 Dbi Trh Nppa Agrp Nampt Agt Nmu Th Cnp Npb Gast Crh Nxph3 Nppc Ghrh Kiss1 Igf1 Nmb Npvf Npff Grp Oxt Calca Rln1 Galp Gnrh1 Vip Apln
CellCount
3000
2000
1000
0 1000 2000 3000
Cell Count
Ranks of Cell Counts
Receptors
Ntrk2 Gpr162 Igf1r Glud1 Ghr Oprm1 Calcr Adcyap1r1 Hcrtr2 Npr2 Lepr Insr Prlr Esr1 Ar Igf2r Oprl1 Adipor1 Trhr Pgr Vipr2 Npy5r Npsr1 Rxfp1 Mchr1 Crhr2 Oprd1 Sstr1 Npffr1 Tacr1 Pth1r Calcrl Npy1r Npr3 Crhr1 Adipor2 Sstr2 Oprk1 Kiss1r Gipr Galr1 Pth2r Sstr3 Paqr8 Ntsr1 Esr2 C3ar1 Avpr1a Cckbr Sstr4 Hcrtr1 Glp1r Glp2r Ednra Grpr Ntsr2 Cckar Mlnr Ednrb Npr1 Rxfp2 Nmur2 Npffr2 Mc4r Oxtr
CellCount
3000
2000
1000
0 1000 2000 3000
Cell Count
C
Top20 subclusters (O vs Y)
Gnrh1 0.623
Tac1 0.582
Cbln2 0.557
Nucb2 0.552
Scg2 0.547
Crh 0.547
Igf1 0.544
Nxph3 0.539
Adcyap1 0.539
Bdnf 0.538
Trh 0.537
Cnp 0.533
Oxt 0.532
Chgb 0.529
Pomc 0.526
Gast 0.526
Penk 0.525
Agt 0.523
Tac3 0.522
Apln 0.522
0.50 0.55 0.60 0.65
AUC
Top20 subclusters (O.T vs Y)
Calca 0.578
Gnrh1 0.575
Scg3 0.546
Agrp 0.543
Nmb 0.538
Igf2 0.537
Prlh 0.533
Nxph4 0.533
Nampt 0.532
Pmch 0.531
Nucb2 0.528
Cbln4 0.528
Hcrt 0.526
Vip 0.524
Nppc 0.524
Npb 0.523
Rln1 0.522
Oxt 0.522
Gast 0.522
Npff 0.522
0.500 0.525 0.550 0.575 0.600
AUC
Top20 subclusters (O.T vs O)
Sct 0.623
Kiss1 0.553
Scg2 0.552
Agt 0.547
Dbi 0.543
Grp 0.536
Nampt 0.533
Igf1 0.532
Vip 0.527
Nmb 0.527
Hcrt 0.527
Oxt 0.524
Cartpt 0.524
Cck 0.523
Pnoc 0.522
Agrp 0.522
Nmu 0.520
Cbln4 0.519
Nucb2 0.518
Npff 0.518
0.50 0.55 0.60 0.65
AUC
D
Top20 subclusters (O vs Y)
Insr 0.594
Npy2r 0.587
Ghsr 0.568
Rxfp3 0.567
Ar 0.562
Gpr162 0.560
Trhr 0.554
Ednra 0.553
Glp1r 0.548
Npr3 0.547
Esr1 0.546
Npy1r 0.543
Calcr 0.542
Gipr 0.541
Hcrtr2 0.539
Glud1 0.539
Rxfp2 0.538
Oprl1 0.537
Nmur2 0.531
Npr1 0.528
0.500 0.525 0.550 0.575 0.600
AUC
Top20 subclusters (O.T vs Y)
Insr 0.598
Ednra 0.573
Ednrb 0.568
Trhr 0.558
Npy5r 0.552
Sctr 0.544
Sstr3 0.542
Oprk1 0.539
Pth2r 0.532
Sstr2 0.531
Ntsr1 0.529
Oprd1 0.528
Vipr2 0.527
Ntsr2 0.527
Galr1 0.527
Pgr 0.526
Npr3 0.524
Npr2 0.523
Crhr1 0.523
Ghr 0.522
0.500 0.525 0.550 0.575 0.600 0.625
AUC
Top20 subclusters (O.T vs O)
Adipor2 0.569
Mlnr 0.555
Hcrtr1 0.551
Nmur2 0.548
Insr 0.547
Npy1r 0.541
Ghr 0.539
Paqr8 0.538
Gipr 0.536
Npr2 0.534
Sstr3 0.533
Cckar 0.532
Oprm1 0.528
Glp1r 0.528
Rxfp1 0.527
Ntsr2 0.527
Lepr 0.527
Oprd1 0.527
Npsr1 0.527
Grpr 0.526
0.500 0.525 0.550 0.575
AUC

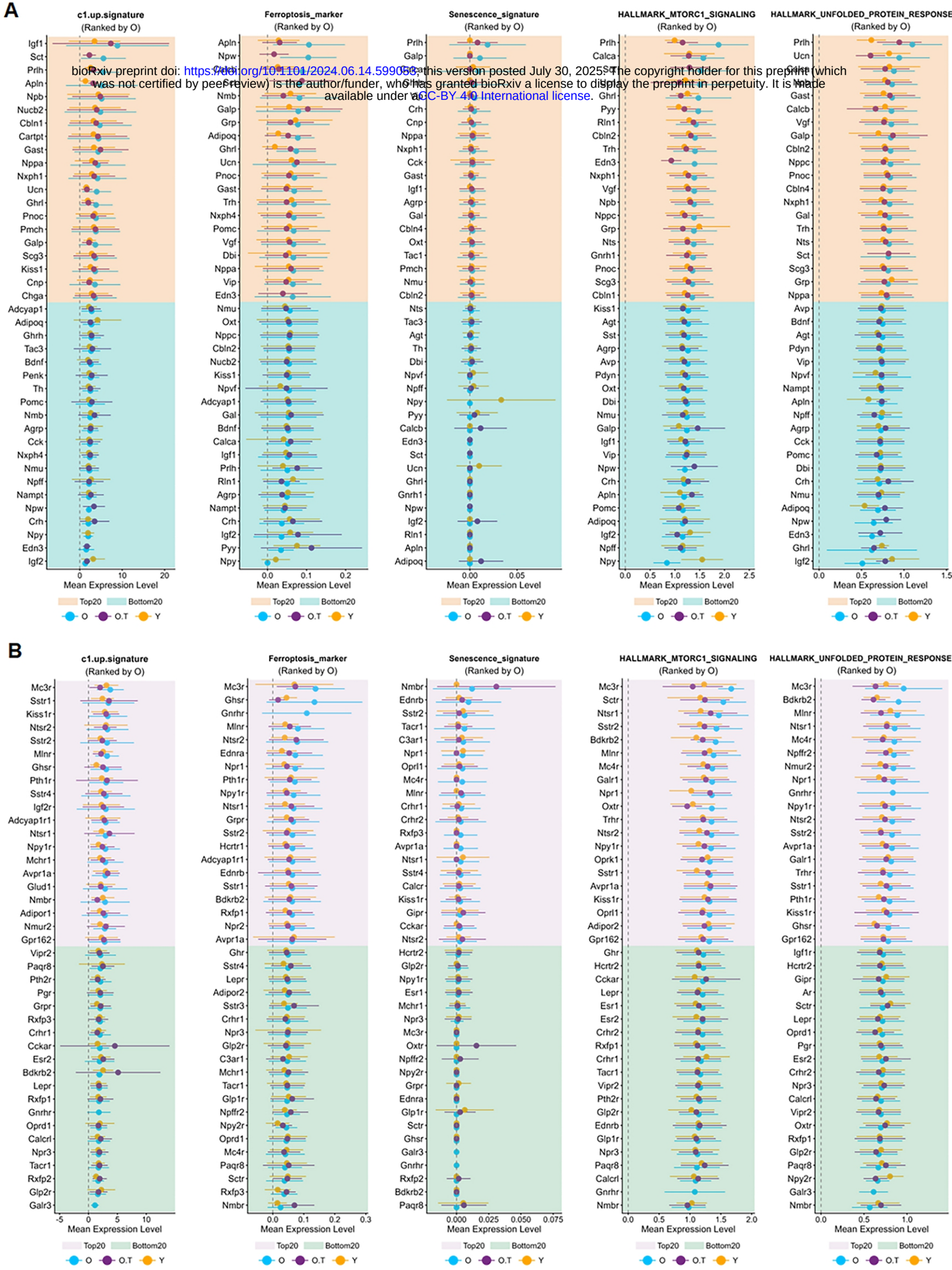

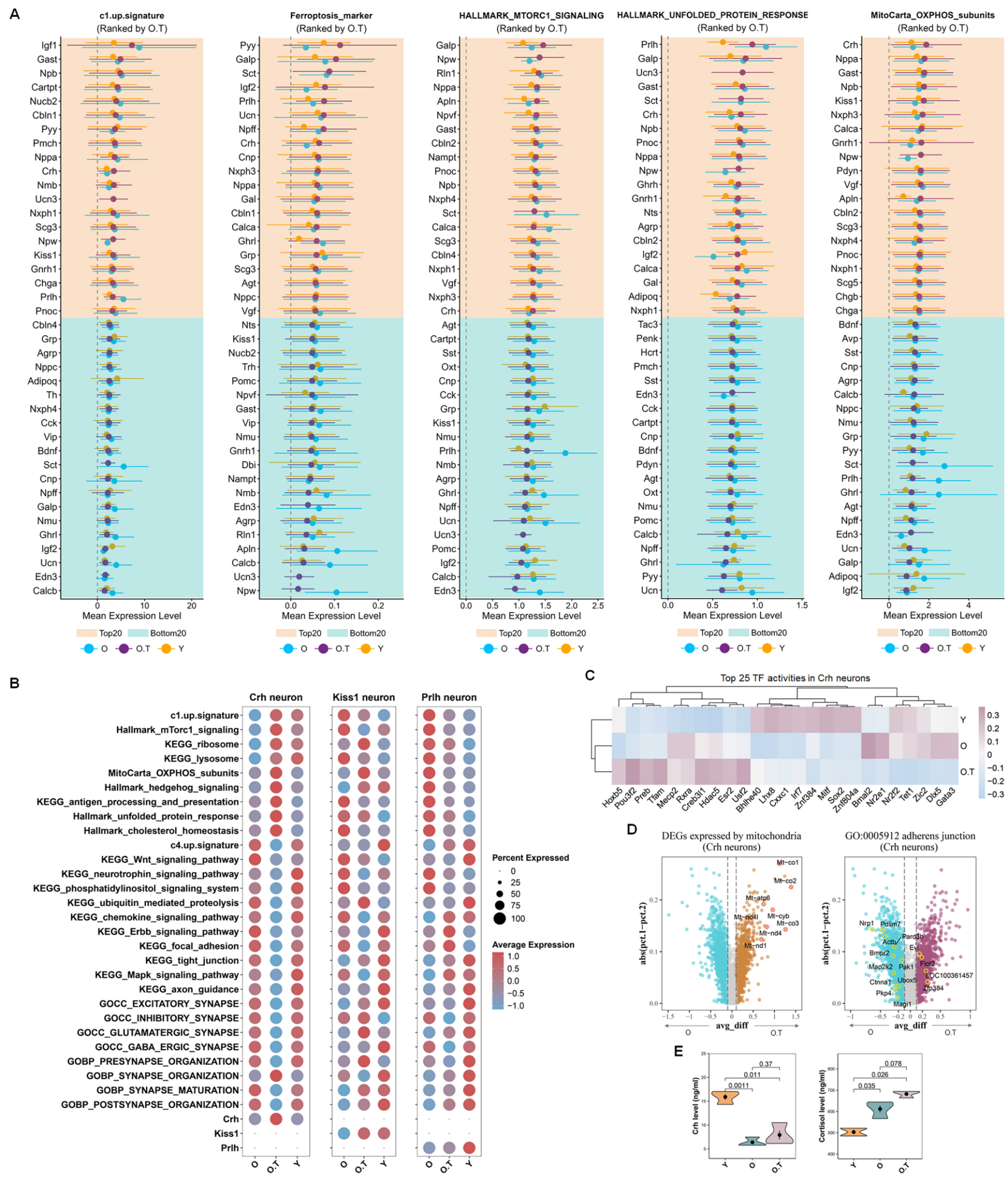
A
c1.up.signature
(Ranked by O.T)
Ferroptosis_marker
(Ranked by O.T)
HALLMARK_MTORC1_SIGNALING
(Ranked by O.T)
HALLMARK_UNFOLDED_PROTEIN_RESPONSE
(Ranked by O.T)
MitoCarta_OXPHOS_subunits
(Ranked by O.T)
Mean Expression Level
Top20
Bottom20
O
O.T
Y
B
Crh neuron
Kiss1 neuron
Prlh neuron
c1.up.signature
Hallmark_mTorc1_signaling
KEGG_ribosome
KEGG_lysosome
MitoCarta_OXPHOS_subunits
Hallmark_hedgehog_signaling
KEGG_antigen_processing_and_presentation
Hallmark_unfolded_protein_response
Hallmark_cholesterol_homeostasis
c4.up.signature
KEGG_Wnt_signaling_pathway
KEGG_neurotrophin_signaling_pathway
KEGG_phosphatidylinositol_signaling_system
KEGG_ubiquitin_mediated_proteolysis
KEGG_chemokine_signaling_pathway
KEGG_Erbb_signaling_pathway
KEGG_focal_adhesion
KEGG_tight_junction
KEGG_Mapk_signaling_pathway
KEGG_axon_guidance
GOCC_EXCITATORY_SYNAPSE
GOCC_INHIBITORY_SYNAPSE
GOCC_GLUTAMATERGIC_SYNAPSE
GOCC_GABA_ERGIC_SYNAPSE
GOBP_PRESYNAPSE_ORGANIZATION
GOBP_SYNAPSE_ORGANIZATION
GOBP_SYNAPSE_MATURATION
GOBP_POSTSYNAPSE_ORGANIZATION
Crh
Kiss1
Prlh
Percent Expressed
Average Expression
C
Top 25 TF activities in Crh neurons
Hoxb5
Pou3f2
Preb
Tfam
Mecp2
Rxra
Creb3l1
Hdac5
Esr2
Usf2
Bhlhe40
Lhx8
Cxxc1
Irf7
Znf384
Mitf
Sox2
Znf804a
Bmal2
Nr2e1
Nr2f2
Tet1
Zic2
Dlx5
Gata3
D
DEGs expressed by mitochondria
(Crh neurons)
GO:0005912 adherens junction
(Crh neurons)
abs(pct.1−pct.2)
avg_diff
E
Crh level (ng/ml)
Cortisol level (ng/ml)

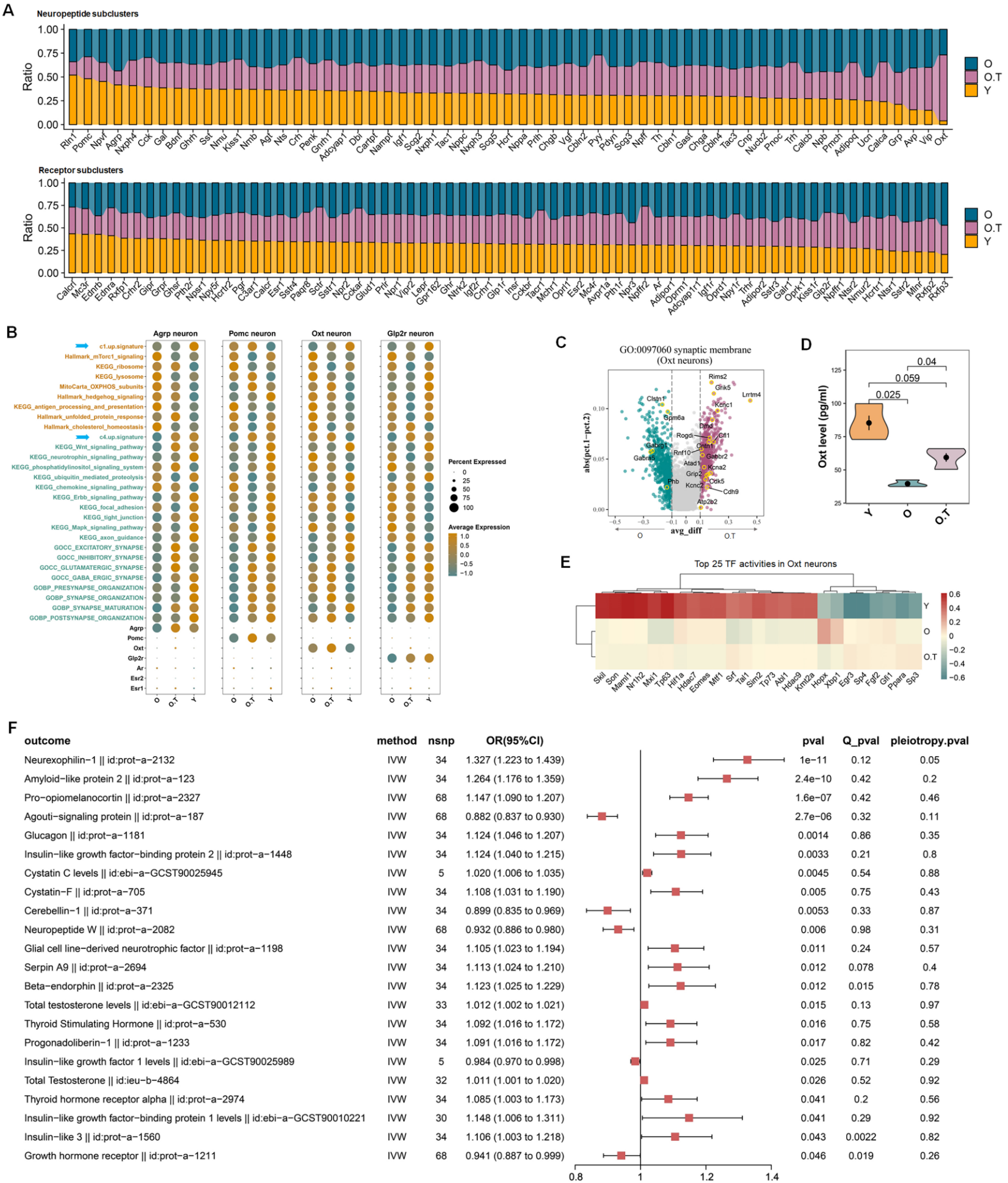

F

outcome	method	nsnp	OR(95%CI)	pval	Q_pval	pleiotropy.pval
Neurexophilin−1 || id:prot−a−2132	IVW	34	1.327 (1.223 to 1.439)	1e−11	0.12	0.05
Amyloid−like protein 2 || id:prot−a−123	IVW	34	1.264 (1.176 to 1.359)	2.4e−10	0.42	0.2
Pro−opiomelanocortin || id:prot−a−2327	IVW	68	1.147 (1.090 to 1.207)	1.6e−07	0.42	0.46
Agouti−signaling protein || id:prot−a−187	IVW	68	0.882 (0.837 to 0.930)	2.7e−06	0.32	0.11
Glucagon || id:prot−a−1181	IVW	34	1.124 (1.046 to 1.207)	0.0014	0.86	0.35
Insulin−like growth factor−binding protein 2 || id:prot−a−1448	IVW	34	1.124 (1.040 to 1.215)	0.0033	0.21	0.8
Cystatin C levels || id:ebi−a−GCST90025945	IVW	5	1.020 (1.006 to 1.035)	0.0045	0.54	0.88
Cystatin−F || id:prot−a−705	IVW	34	1.108 (1.031 to 1.190)	0.005	0.75	0.43
Cerebellin−1 || id:prot−a−371	IVW	34	0.899 (0.835 to 0.969)	0.0053	0.33	0.87
Neuropeptide W || id:prot−a−2082	IVW	68	0.932 (0.886 to 0.980)	0.006	0.98	0.31
Glial cell line−derived neurotrophic factor || id:prot−a−1198	IVW	34	1.105 (1.023 to 1.194)	0.011	0.24	0.57
Serpin A9 || id:prot−a−2694	IVW	34	1.113 (1.024 to 1.210)	0.012	0.078	0.4
Beta−endorphin || id:prot−a−2325	IVW	34	1.123 (1.025 to 1.229)	0.012	0.015	0.78
Total testosterone levels || id:ebi−a−GCST90012112	IVW	33	1.012 (1.002 to 1.021)	0.015	0.13	0.97
Thyroid Stimulating Hormone || id:prot−a−530	IVW	34	1.092 (1.016 to 1.172)	0.016	0.75	0.58
Progonadoliberin−1 || id:prot−a−1233	IVW	34	1.091 (1.016 to 1.172)	0.017	0.82	0.42
Insulin−like growth factor 1 levels || id:ebi−a−GCST90025989	IVW	5	0.984 (0.970 to 0.998)	0.025	0.71	0.29
Total Testosterone || id:ieu−b−4864	IVW	32	1.011 (1.001 to 1.020)	0.026	0.52	0.92
Thyroid hormone receptor alpha || id:prot−a−2974	IVW	34	1.085 (1.003 to 1.173)	0.041	0.2	0.56
Insulin−like growth factor−binding protein 1 levels || id:ebi−a−GCST90010221	IVW	30	1.148 (1.006 to 1.311)	0.041	0.29	0.92
Insulin−like 3 || id:prot−a−1560	IVW	34	1.106 (1.003 to 1.218)	0.043	0.0022	0.82
Growth hormone receptor || id:prot−a−1211	IVW	68	0.941 (0.887 to 0.999)	0.046	0.019	0.26

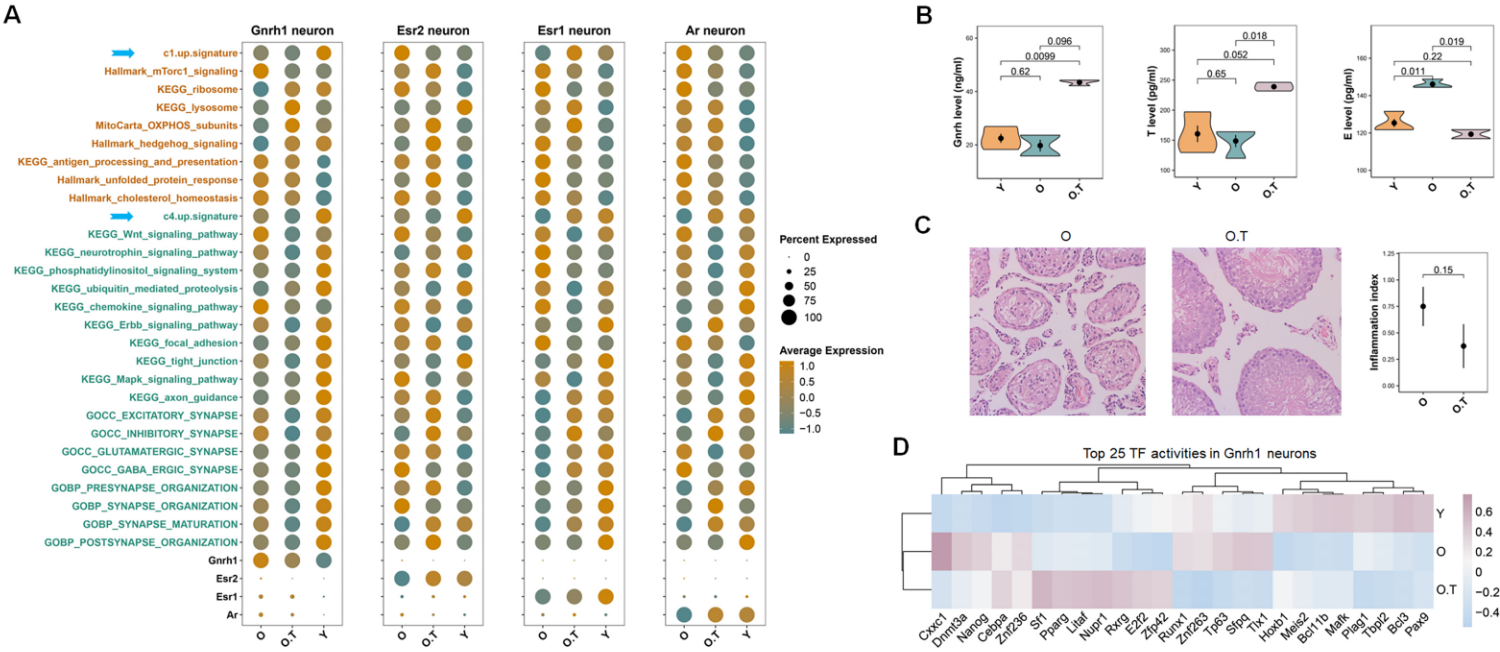

F

exposure	outcome	method	nsnp	OR(95%CI)	pval	Q_pval	pleiotropy.pval
GNRH1	Proenkephalin−A || id:prot−a−2247	IVW	48	1.336 (1.264 to 1.413)	1.9e−24	0.72	0.26
GNRH1	Proprotein convertase subtilisin/kexin type 7 || id:prot−a−2212	IVW	24	1.254 (1.159 to 1.357)	1.8e−08	0.51	0.95
GNRH1	Agouti−signaling protein || id:prot−a−187	IVW	48	1.218 (1.132 to 1.310)	1.3e−07	0.0015	0.31
GNRH1	Growth hormone receptor || id:prot−a−1211	IVW	48	0.863 (0.816 to 0.913)	2.3e−07	0.98	0.34
GNRH1	Galanin peptides || id:prot−a−1166	IVW	24	1.236 (1.133 to 1.349)	1.9e−06	0.2	0.93
GNRH1	Estrogen receptor || id:prot−a−991	IVW	24	1.222 (1.124 to 1.329)	2.8e−06	0.3	0.73
GNRH1	Pro−opiomelanocortin || id:prot−a−2327	IVW	48	1.139 (1.077 to 1.204)	4.8e−06	0.98	0.083
GNRH1	Insulin−like growth factor−binding protein 6 || id:prot−a−1450	IVW	24	1.232 (1.124 to 1.351)	8.7e−06	0.11	0.67
GNRH1	Beta−endorphin || id:prot−a−2325	IVW	24	1.184 (1.094 to 1.281)	0.000027	0.55	0.48
GNRH1	Brain−derived neurotrophic factor || id:prot−a−242	IVW	24	1.131 (1.045 to 1.223)	0.0022	0.63	0.91
GNRH1	Adrenomedullin || id:prot−a−48	IVW	24	1.271 (1.083 to 1.492)	0.0033	9.3e−11	0.72
GNRH1	Insulin−like growth factor−binding protein 1 levels || id:ebi−a−GCST90010221	IVW	22	0.820 (0.718 to 0.936)	0.0034	0.28	0.57
GNRH1	Prolactin receptor || id:prot−a−2377	IVW	24	1.124 (1.039 to 1.216)	0.0036	0.85	0.44
GNRH1	Insulin−like growth factor−binding protein 3 || id:prot−a−1449	IVW	24	0.883 (0.811 to 0.962)	0.0044	0.25	0.63
GNRH1	Early placenta insulin−like peptide || id:prot−a−1561	IVW	24	1.117 (1.032 to 1.208)	0.0059	0.58	0.58
GNRH1	Bradykinin, des−arg(9) || id:met−a−656	IVW	10	0.778 (0.641 to 0.943)	0.01	4.6e−31	0.071
GNRH1	Leptin receptor || id:prot−a−1724	IVW	24	1.097 (1.014 to 1.187)	0.021	0.98	0.42
GNRH1	Thyroid hormone receptor alpha || id:prot−a−2974	IVW	24	1.086 (1.004 to 1.176)	0.039	0.82	0.78

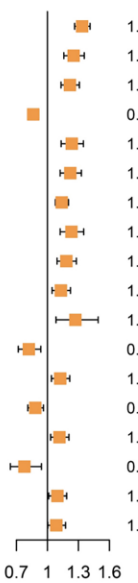

G

exposure	outcome	method	nsnp	OR(95%CI)	pval	Q_pval	pleiotropy.pval
GNRH1	Somatostatin−28 || id:prot−a−2846	IVW	24	1.598 (1.468 to 1.740)	4.1e−27	0.26	0.53
GNRH1	Chromogranin−A || id:prot−a−538	IVW	24	1.650 (1.499 to 1.816)	1.7e−24	0.06	0.5
GNRH1	Neuropeptide W || id:prot−a−2082	IVW	48	1.552 (1.407 to 1.711)	1.3e−18	4.8e−12	0.77
GNRH1	Protachykinin−1 || id:prot−a−2920	IVW	24	1.596 (1.421 to 1.791)	2.3e−15	0.001	0.89
GNRH1	Glucagon || id:prot−a−1181	IVW	24	1.609 (1.414 to 1.830)	4.5e−13	0.000021	0.98
GNRH1	Brain natriuretic peptide 32 || id:prot−a−2077	IVW	48	1.223 (1.157 to 1.294)	1.3e−12	0.9	0.026
GNRH1	Corticotropin || id:prot−a−2326	IVW	24	1.221 (1.129 to 1.322)	6.4e−07	0.79	0.73
GNRH1	Prolactin−releasing peptide || id:prot−a−2376	IVW	24	1.219 (1.126 to 1.320)	1.1e−06	0.43	0.089
GNRH1	Progonadoliberin−2 || id:prot−a−1234	IVW	24	1.228 (1.125 to 1.340)	4e−06	0.21	0.42
GNRH1	Secretogranin−1 || id:prot−a−539	IVW	24	1.178 (1.089 to 1.274)	0.000046	0.81	0.51
GNRH1	Atrial natriuretic factor || id:prot−a−2076	IVW	24	1.155 (1.068 to 1.250)	0.00032	0.57	0.56
GNRH1	Estradiol 17−beta−dehydrogenase 2 || id:prot−a−1383	IVW	24	1.135 (1.049 to 1.228)	0.0016	0.69	0.62
GNRH1	Insulin−like growth factor I || id:prot−a−1443	IVW	24	0.896 (0.828 to 0.970)	0.0063	0.95	0.48
GNRH1	Insulin−like growth factor 1 receptor || id:prot−a−1444	IVW	24	1.090 (1.003 to 1.184)	0.042	0.33	0.62